Constructing robust high order entropy stable discontinuous Galerkin methods

Jesse Chan

Dept. of Computational Applied Mathematics and Operations Research
Rice University

Department of Mathematics, The Ohio State University

Collaborators

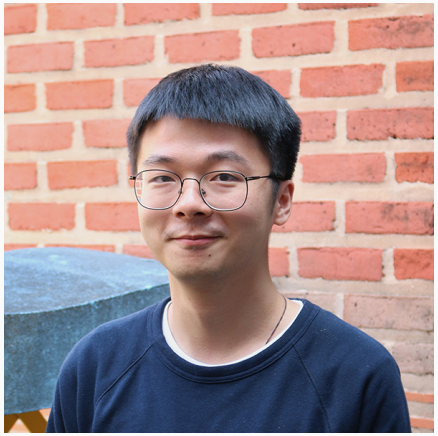

Yimin Lin (Euler, compressible NS)

Ignacio Tomas

Tim Warburton

Hendrik Ranocha

Andres Ruéda-Ramírez

Gregor Gassner

High order finite element methods for hyperbolic PDEs

- Aerodynamics applications: acoustics, vorticular flows, turbulence, shocks.
- Goal: high accuracy on unstructured meshes.
- Discontinuous Galerkin (DG) methods: geometric flexibility + high order.

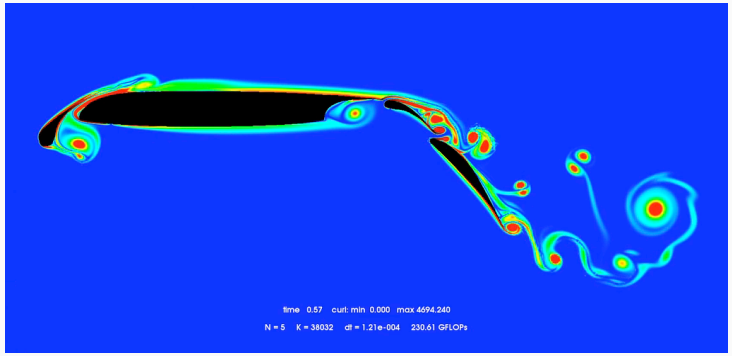

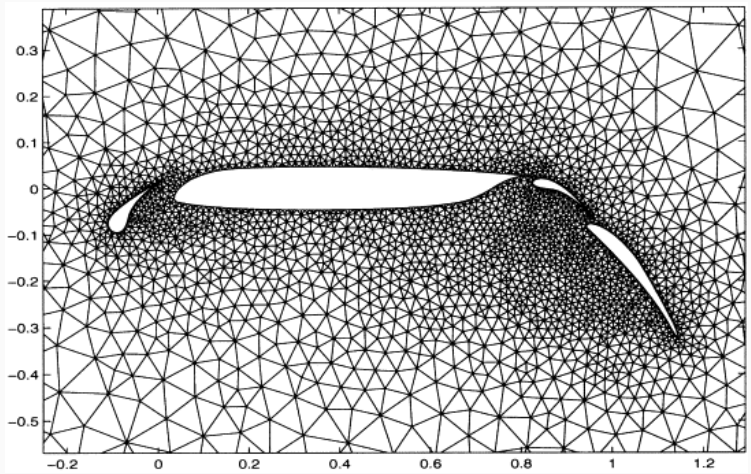

Mesh from Slawig 2001.

High order finite element methods for hyperbolic PDEs

- Aerodynamics applications: acoustics, vorticular flows, turbulence, shocks.
- Goal: high accuracy on unstructured meshes.
- Discontinuous Galerkin (DG) methods: geometric flexibility + high order.

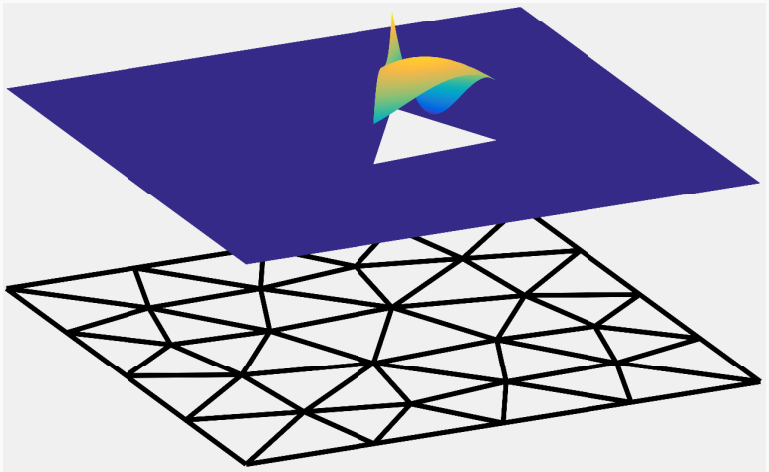

Why discontinuous Galerkin methods?

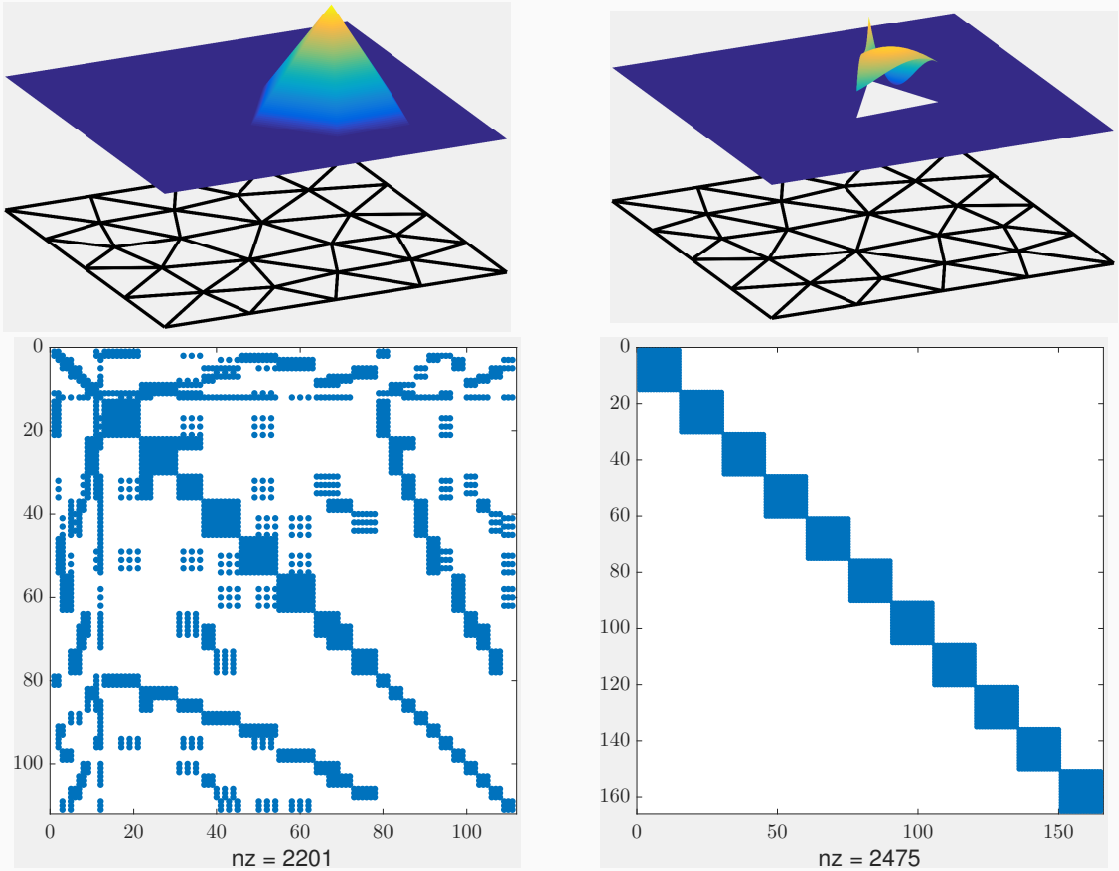

(a) High order FEM **(b)** High order DG

High order DG mass matrices: easily invertible for explicit time-stepping.

Why high order accuracy?

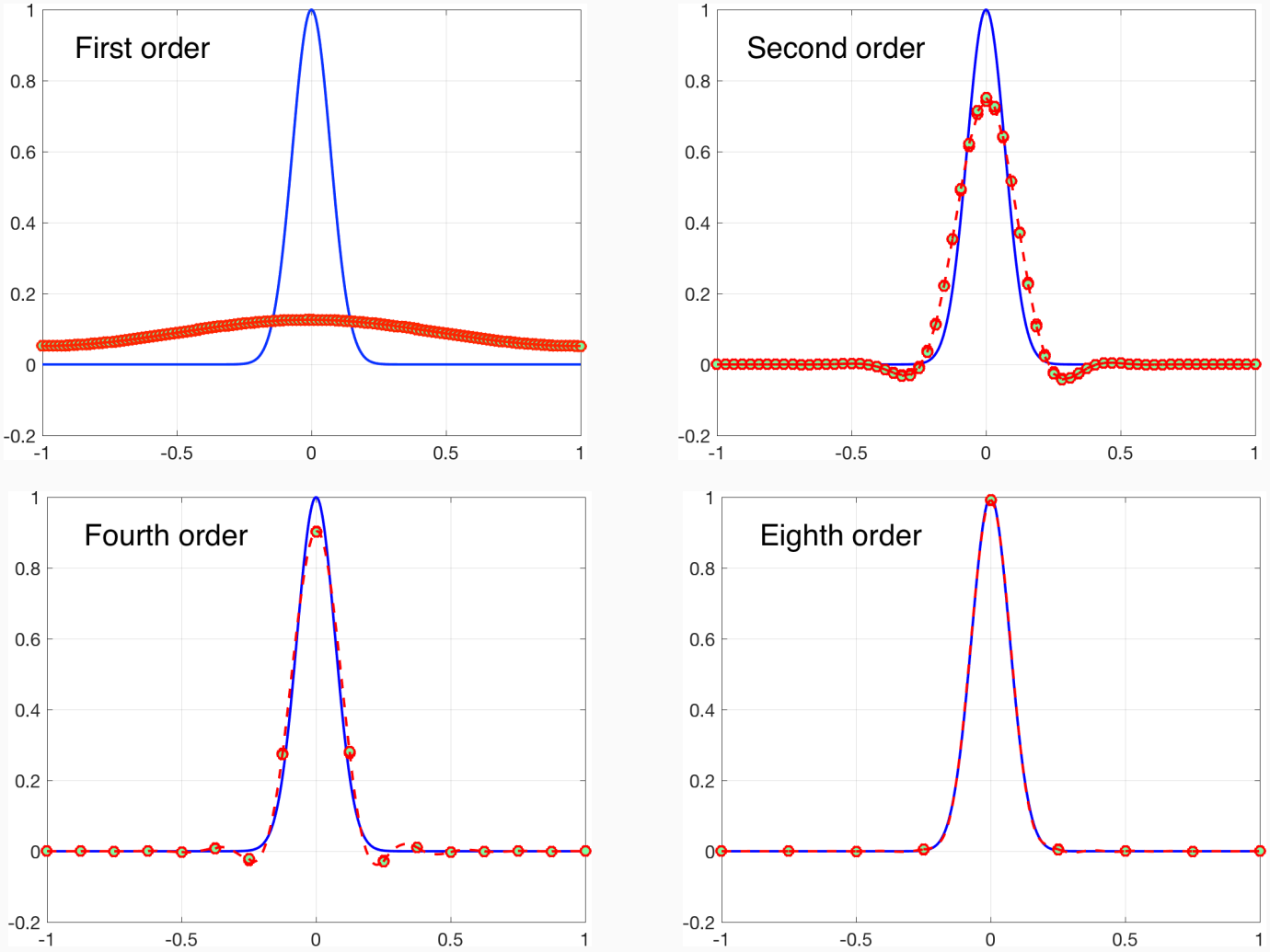

Accurate resolution of propagating vortices and waves.

Why high order accuracy?

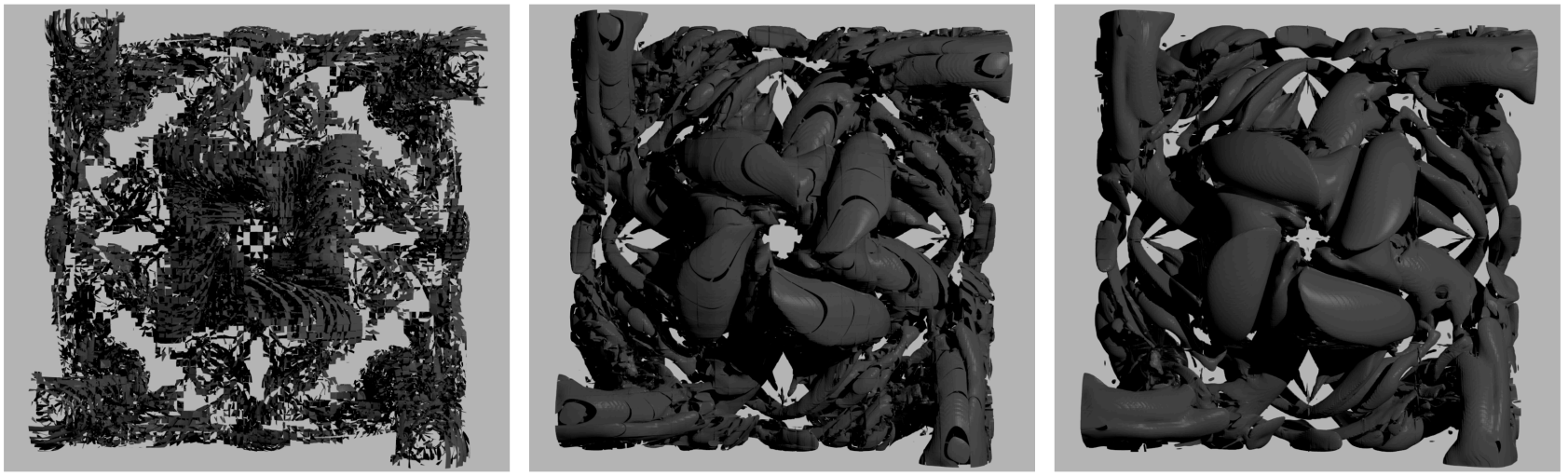

2nd, 4th, and 16th order Taylor-Green vortex. Vorticular structures and acoustic waves are both sensitive to numerical dissipation.

Results from Beck and Gassner (2013).

Why *not* high order DG methods?

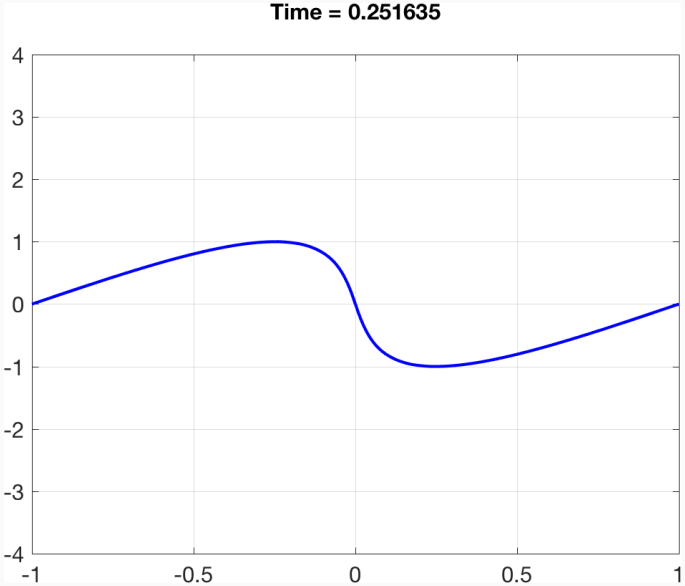

(a) Exact solution

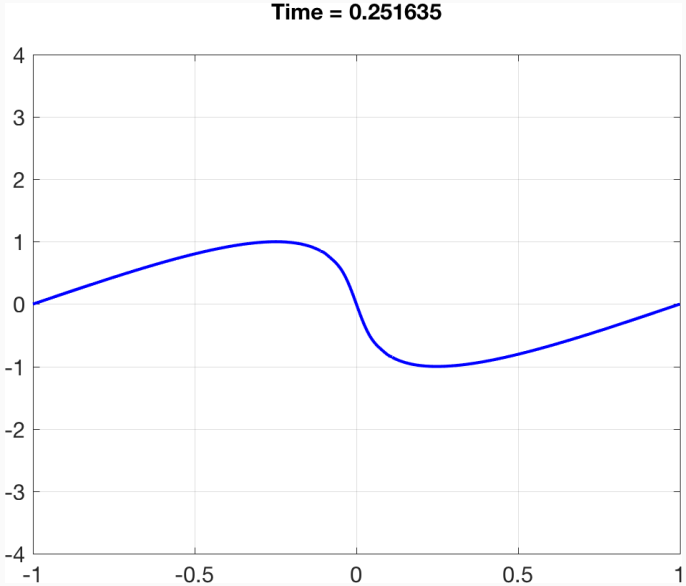

(b) 8th order DG

High order methods blow up for under-resolved solutions of nonlinear conservation laws (e.g., shocks and turbulence).

Why *not* high order DG methods?

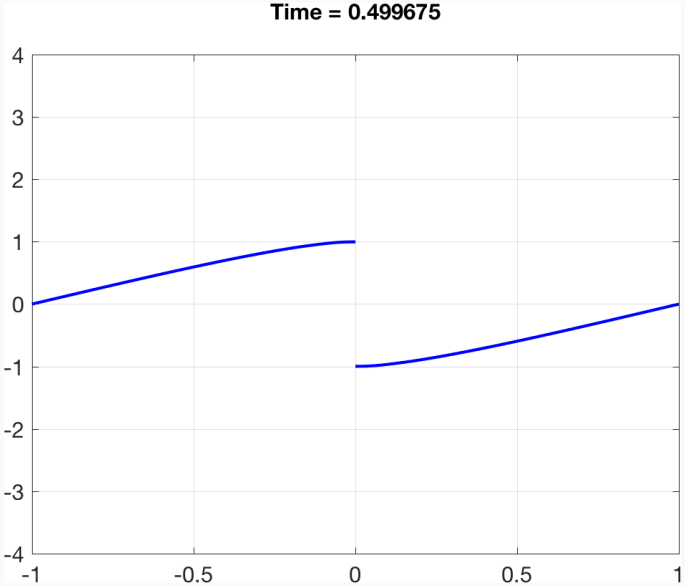

(a) Exact solution

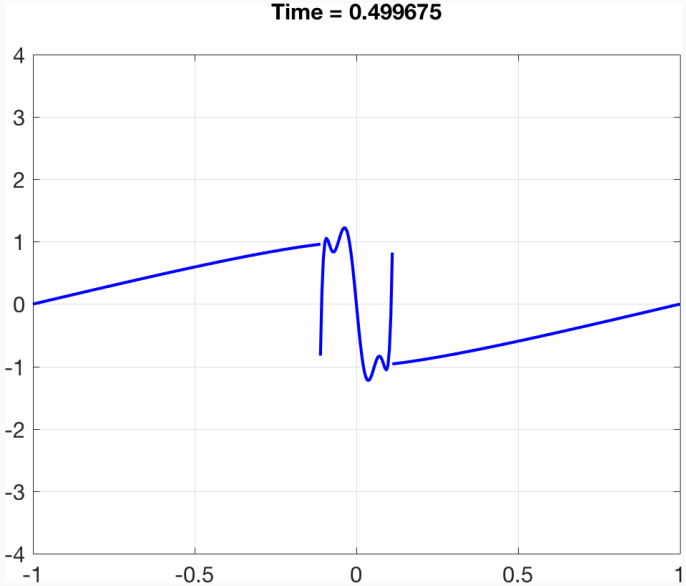

(b) 8th order DG

High order methods blow up for under-resolved solutions of nonlinear conservation laws (e.g., shocks and turbulence).

Why *not* high order DG methods?

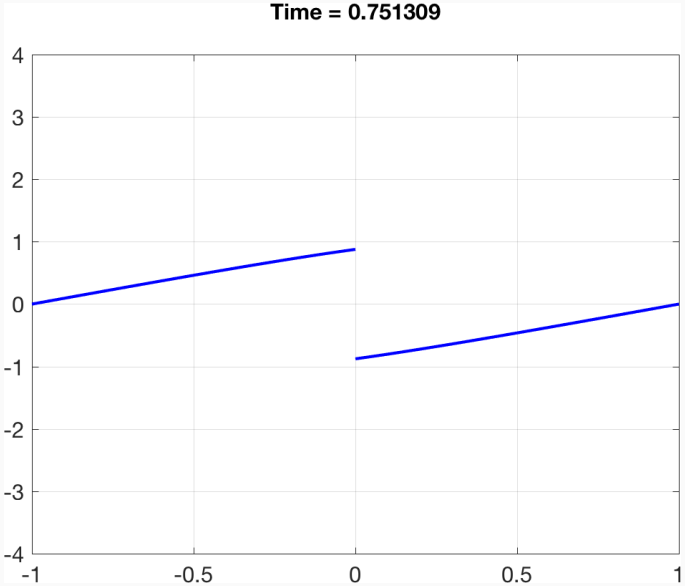

(a) Exact solution

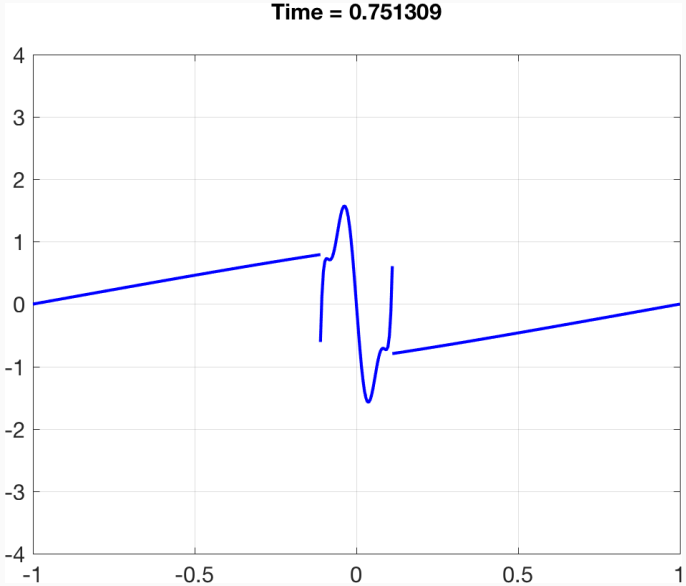

(b) 8th order DG

High order methods blow up for under-resolved solutions of nonlinear conservation laws (e.g., shocks and turbulence).

Why *not* high order DG methods?

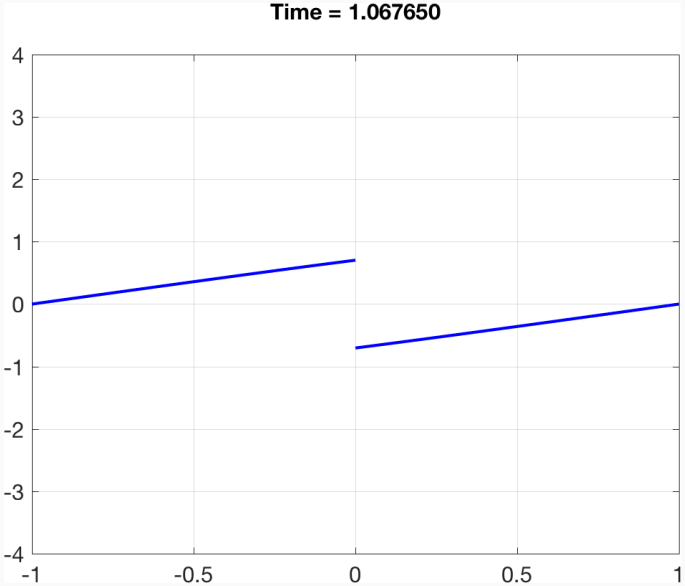

(a) Exact solution

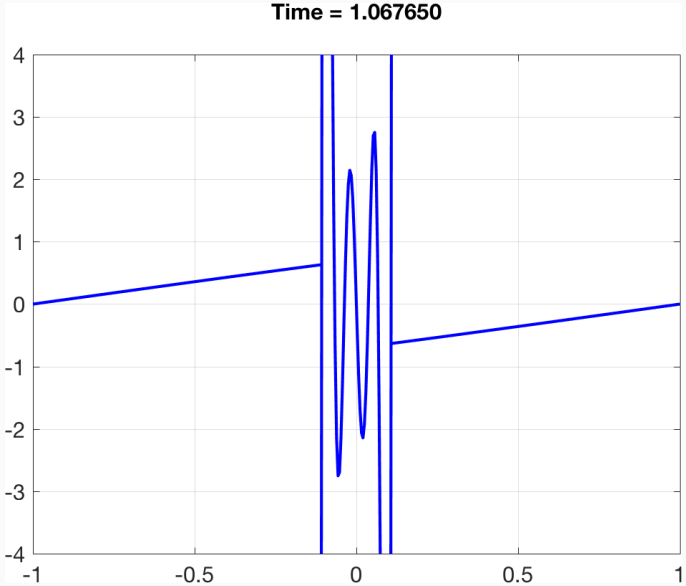

(b) 8th order DG

High order methods blow up for under-resolved solutions of nonlinear conservation laws (e.g., shocks and turbulence).

Why entropy stability for high order schemes?

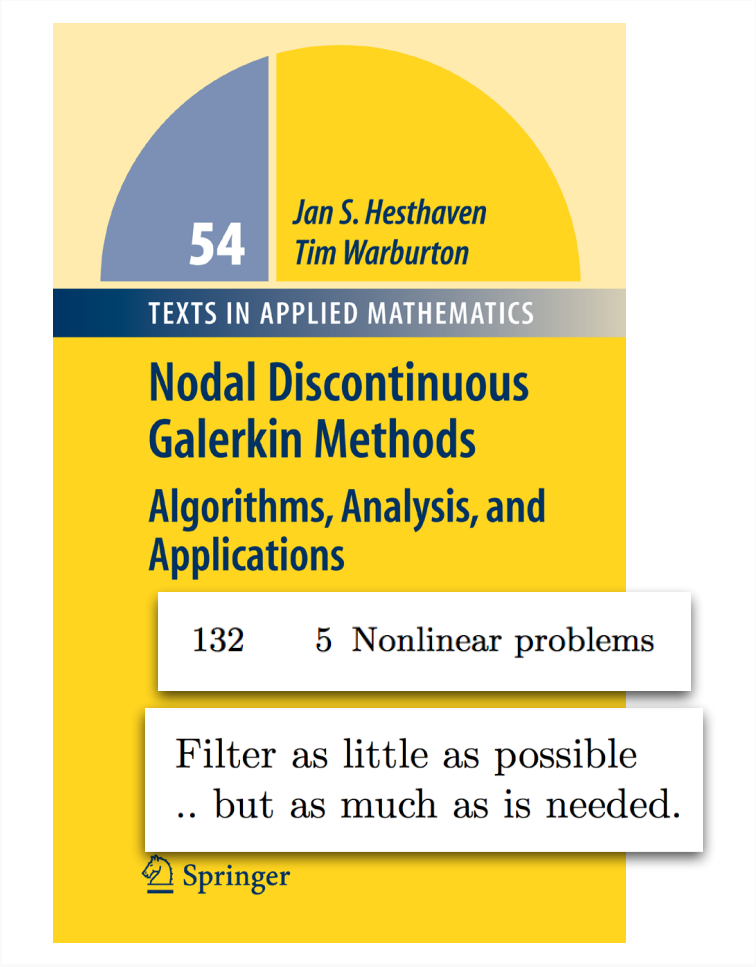

- High order DG needs heuristic stabilization (e.g., artificial viscosity, filtering).
- Entropy stable schemes improve robustness without *no added dissipation*.
- Turns DG into a "good" high order method (though not 100% bulletproof).

Finite volume methods: Tadmor, Chandrashekar, Ray, Svard, Fjordholm, Mishra, LeFloch, Rohde, ...

High order tensor product elements: Fisher, Carpenter, Gassner, Winters, Kopriva, Persson, ...

High order general elements: Chen and Shu, Crean, Hicken, Del Rey Fernandez, Zingg, ...

Examples of high order entropy stable simulations

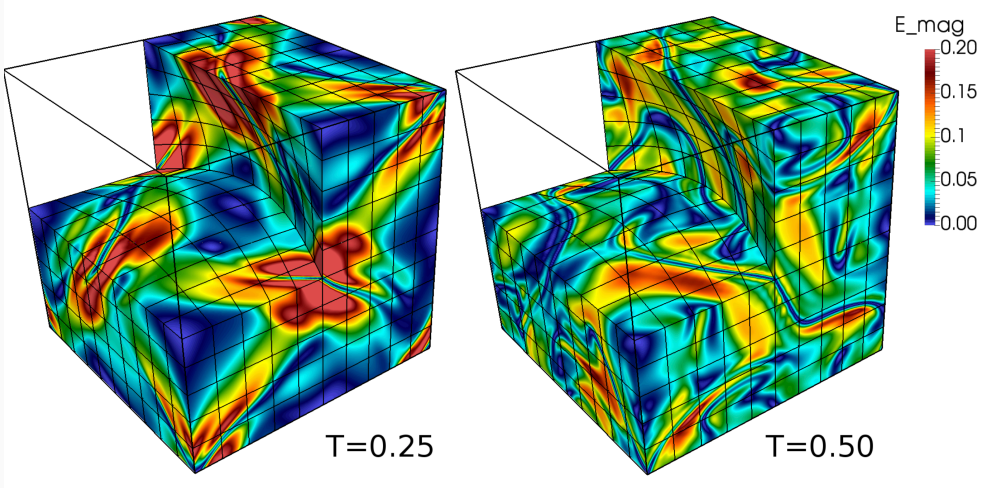

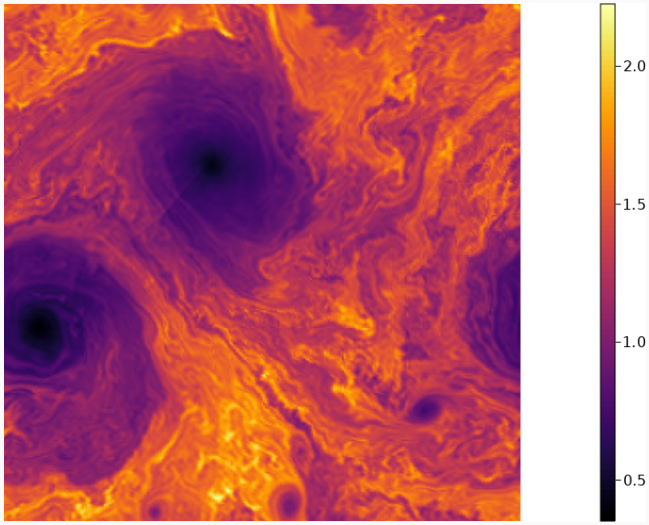

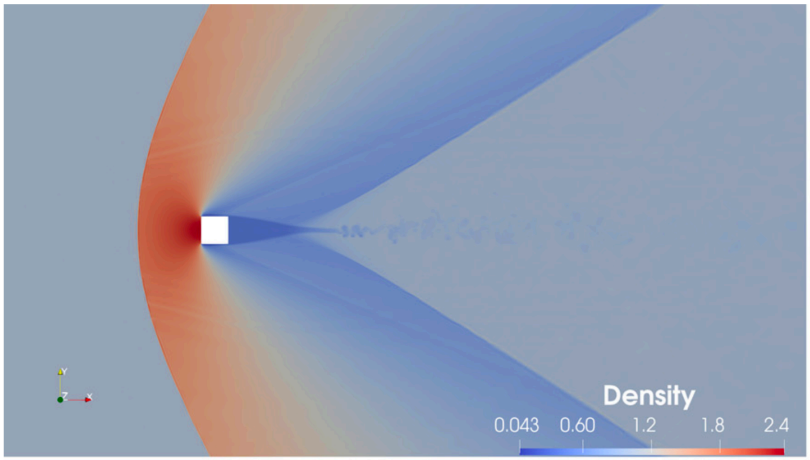

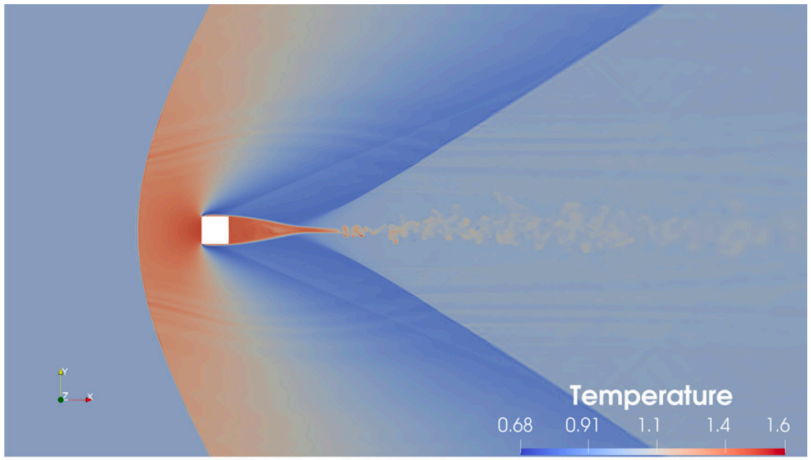

All simulations are ESDG without artificial viscosity, filtering, or slope limiting.

Bohm et al. (2019). *An entropy stable nodal DG method for the resistive MHD equations. Part I.*

Dalcin et al. (2019). *Conservative and ES solid wall BCs for the compressible NS equations.*

Talk outline

1. From entropy stable finite volumes to entropy stable nodal DG

2. Positivity preserving entropy stable nodal DG for the compressible Navier-Stokes equations (Yimin Lin)

3. "Modal" entropy stable DG formulations

From entropy stable finite volumes to entropy stable nodal DG

Entropy stability for nonlinear problems

- Energy balance for nonlinear conservation laws (Burgers', shallow water, compressible Euler + Navier-Stokes).

$$\frac{\partial \boldsymbol{u}}{\partial t} + \frac{\partial \boldsymbol{f}(\boldsymbol{u})}{\partial x} = 0.$$

- Continuous entropy inequality: convex entropy function $S(\boldsymbol{u})$, "entropy potential" $\psi(\boldsymbol{u})$, entropy variables $\boldsymbol{v}(\boldsymbol{u})$

$$\int_\Omega \boldsymbol{v}^T \left(\frac{\partial \boldsymbol{u}}{\partial t} + \frac{\partial \boldsymbol{f}(\boldsymbol{u})}{\partial x} \right) = 0, \qquad \boxed{\boldsymbol{v}(\boldsymbol{u}) = \frac{\partial S}{\partial \boldsymbol{u}}}$$

$$\implies \int_\Omega \frac{\partial S(\boldsymbol{u})}{\partial t} + \left(\boldsymbol{v}^T \boldsymbol{f}(\boldsymbol{u}) - \psi(\boldsymbol{u}) \right) \Big|_{-1}^{1} \leq 0.$$

Entropy conservative finite volume methods

- Finite volume scheme:

$$\frac{\mathrm{d}\mathbf{u}_i}{\mathrm{dt}} + \frac{\boldsymbol{f}_S(\mathbf{u}_{i+1}, \mathbf{u}_i) - \boldsymbol{f}_S(\mathbf{u}_{i+1}, \mathbf{u}_i)}{h} = \mathbf{0}.$$

- Take $\boldsymbol{f}_S$ to be an entropy conservative numerical flux

$$\begin{aligned} \boldsymbol{f}_S(\boldsymbol{u}, \boldsymbol{u}) &= \boldsymbol{f}(\boldsymbol{u}), && \text{(consistency)} \\ \boldsymbol{f}_S(\boldsymbol{u}, \boldsymbol{v}) &= \boldsymbol{f}_S(\boldsymbol{v}, \boldsymbol{u}), && \text{(symmetry)} \\ (\boldsymbol{v}_L - \boldsymbol{v}_R)^T \boldsymbol{f}_S(\boldsymbol{u}_L, \boldsymbol{u}_R) &= \psi_L - \psi_R, && \text{(conservation).} \end{aligned}$$

- Can show numerical scheme conserves entropy

$$\int_\Omega \frac{\partial S(\boldsymbol{u})}{\partial t} \approx \sum_i h \frac{\mathrm{d}S(\mathbf{u}_i)}{\mathrm{dt}} = 0.$$

Tadmor (1987). *The numerical viscosity of entropy stable schemes for systems of conservation laws.*

Entropy stable finite volume methods

- Finite volume scheme with dissipation term $\mathbf{d}(\mathbf{u})$:

$$\frac{\mathrm{d}\mathbf{u}_i}{\mathrm{dt}} + \frac{\boldsymbol{f}_S(\mathbf{u}_{i+1}, \mathbf{u}_i) - \boldsymbol{f}_S(\mathbf{u}_{i+1}, \mathbf{u}_i)}{h} = \mathbf{d}(\mathbf{u}).$$

- Take $\boldsymbol{f}_S$ to be an entropy conservative numerical flux

$$\begin{aligned} \boldsymbol{f}_S(\boldsymbol{u}, \boldsymbol{u}) &= \boldsymbol{f}(\boldsymbol{u}), && \text{(consistency)} \\ \boldsymbol{f}_S(\boldsymbol{u}, \boldsymbol{v}) &= \boldsymbol{f}_S(\boldsymbol{v}, \boldsymbol{u}), && \text{(symmetry)} \\ (\boldsymbol{v}_L - \boldsymbol{v}_R)^T \boldsymbol{f}_S(\boldsymbol{u}_L, \boldsymbol{u}_R) &= \psi_L - \psi_R, && \text{(conservation).} \end{aligned}$$

- Can show numerical scheme dissipates entropy

$$\int_\Omega \frac{\partial S(\boldsymbol{u})}{\partial t} \approx \sum_i h \frac{\mathrm{d}S(\mathbf{u}_i)}{\mathrm{dt}} = \mathbf{v}^T \mathbf{d}(\mathbf{u}) \overset{?}{\leq} 0.$$

Tadmor (1987). *The numerical viscosity of entropy stable schemes for systems of conservation laws.*

Matrix reformulation using Hadamard products

Hadamard product of two matrices $\mathbf{A} \circ \mathbf{B}$

$$\begin{bmatrix} \mathbf{A}_{11} & \dots & \mathbf{A}_{1n} \\ \vdots & \ddots & \vdots \\ \mathbf{A}_{n1} & \dots & \mathbf{A}_{nn} \end{bmatrix} \circ \begin{bmatrix} \mathbf{B}_{11} & \dots & \mathbf{B}_{1n} \\ \vdots & \ddots & \vdots \\ \mathbf{B}_{n1} & \dots & \mathbf{B}_{nn} \end{bmatrix} = \begin{bmatrix} \mathbf{A}_{11}\mathbf{B}_{11} & \dots & \mathbf{A}_{1n}\mathbf{B}_{1n} \\ \vdots & \ddots & \vdots \\ \mathbf{A}_{n1}\mathbf{B}_{n1} & \dots & \mathbf{A}_{nn}\mathbf{B}_{nn} \end{bmatrix}.$$

Rewrite an N-point (periodic) finite volume scheme as

$$\frac{\mathrm{d}}{\mathrm{dt}} \begin{bmatrix} \mathbf{u}_1 \\ \mathbf{u}_2 \\ \vdots \\ \mathbf{u}_N \end{bmatrix} + \frac{1}{h} \begin{bmatrix} f_S(\mathbf{u}_1, \mathbf{u}_2) - f_S(\mathbf{u}_N, \mathbf{u}_1) \\ f_S(\mathbf{u}_2, \mathbf{u}_3) - f_S(\mathbf{u}_1, \mathbf{u}_2) \\ \vdots \\ f_S(\mathbf{u}_N, \mathbf{u}_1) - f_S(\mathbf{u}_{N-1}, \mathbf{u}_N) \end{bmatrix} = \mathbf{0}.$$

Matrix reformulation using Hadamard products

Hadamard product of two matrices $\mathbf{A} \circ \mathbf{B}$

$$\begin{bmatrix} \mathbf{A}_{11} & \dots & \mathbf{A}_{1n} \\ \vdots & \ddots & \vdots \\ \mathbf{A}_{n1} & \dots & \mathbf{A}_{nn} \end{bmatrix} \circ \begin{bmatrix} \mathbf{B}_{11} & \dots & \mathbf{B}_{1n} \\ \vdots & \ddots & \vdots \\ \mathbf{B}_{n1} & \dots & \mathbf{B}_{nn} \end{bmatrix} = \begin{bmatrix} \mathbf{A}_{11}\mathbf{B}_{11} & \dots & \mathbf{A}_{1n}\mathbf{B}_{1n} \\ \vdots & \ddots & \vdots \\ \mathbf{A}_{n1}\mathbf{B}_{n1} & \dots & \mathbf{A}_{nn}\mathbf{B}_{nn} \end{bmatrix}.$$

Rewrite an N-point (periodic) finite volume scheme as

$$\frac{\mathrm{d}}{\mathrm{dt}} \begin{bmatrix} \mathbf{u}_1 \\ \mathbf{u}_2 \\ \vdots \\ \mathbf{u}_N \end{bmatrix} + \frac{1}{h} \begin{bmatrix} \boldsymbol{f}_S(\mathbf{u}_1, \mathbf{u}_2) - \boldsymbol{f}_S(\mathbf{u}_N, \mathbf{u}_1) \\ \boldsymbol{f}_S(\mathbf{u}_2, \mathbf{u}_3) - \boldsymbol{f}_S(\mathbf{u}_1, \mathbf{u}_2) \\ \vdots \\ \boldsymbol{f}_S(\mathbf{u}_N, \mathbf{u}_1) - \boldsymbol{f}_S(\mathbf{u}_{N-1}, \mathbf{u}_N) \end{bmatrix} = \mathbf{0}.$$

Matrix reformulation using Hadamard products

Hadamard product of two matrices $\mathbf{A} \circ \mathbf{B}$

$$\begin{bmatrix} \mathbf{A}_{11} & \dots & \mathbf{A}_{1n} \\ \vdots & \ddots & \vdots \\ \mathbf{A}_{n1} & \dots & \mathbf{A}_{nn} \end{bmatrix} \circ \begin{bmatrix} \mathbf{B}_{11} & \dots & \mathbf{B}_{1n} \\ \vdots & \ddots & \vdots \\ \mathbf{B}_{n1} & \dots & \mathbf{B}_{nn} \end{bmatrix} = \begin{bmatrix} \mathbf{A}_{11}\mathbf{B}_{11} & \dots & \mathbf{A}_{1n}\mathbf{B}_{1n} \\ \vdots & \ddots & \vdots \\ \mathbf{A}_{n1}\mathbf{B}_{n1} & \dots & \mathbf{A}_{nn}\mathbf{B}_{nn} \end{bmatrix}.$$

Rewrite an N-point (periodic) finite volume scheme as

$$h\frac{\mathrm{d}}{\mathrm{dt}} \begin{bmatrix} \mathbf{u}_1 \\ \mathbf{u}_2 \\ \vdots \\ \mathbf{u}_N \end{bmatrix} + \begin{bmatrix} \mathbf{F}_{1,2} - \mathbf{F}_{1,N} \\ \mathbf{F}_{2,3} - \mathbf{F}_{2,1} \\ \vdots \\ \mathbf{F}_{N,1} - \mathbf{F}_{N,N-1} \end{bmatrix} = \mathbf{0}, \qquad \mathbf{F}_{ij} = \boldsymbol{f}_S(\mathbf{u}_i, \mathbf{u}_j).$$

Matrix reformulation using Hadamard products

Hadamard product of two matrices $\mathbf{A} \circ \mathbf{B}$

$$\begin{bmatrix} \mathbf{A}_{11} & \dots & \mathbf{A}_{1n} \\ \vdots & \ddots & \vdots \\ \mathbf{A}_{n1} & \dots & \mathbf{A}_{nn} \end{bmatrix} \circ \begin{bmatrix} \mathbf{B}_{11} & \dots & \mathbf{B}_{1n} \\ \vdots & \ddots & \vdots \\ \mathbf{B}_{n1} & \dots & \mathbf{B}_{nn} \end{bmatrix} = \begin{bmatrix} \mathbf{A}_{11}\mathbf{B}_{11} & \dots & \mathbf{A}_{1n}\mathbf{B}_{1n} \\ \vdots & \ddots & \vdots \\ \mathbf{A}_{n1}\mathbf{B}_{n1} & \dots & \mathbf{A}_{nn}\mathbf{B}_{nn} \end{bmatrix}.$$

Rewrite an N-point (periodic) finite volume scheme as

$$\begin{bmatrix} \mathbf{F}_{1,2} - \mathbf{F}_{1,N} \\ \mathbf{F}_{2,3} - \mathbf{F}_{2,1} \\ \vdots \\ \mathbf{F}_{N,1} - \mathbf{F}_{N,N-1} \end{bmatrix} = \left(\begin{bmatrix} 0 & 1 & & -1 \\ -1 & 0 & 1 & \\ & \ddots & \ddots & 1 \\ 1 & & -1 & 0 \end{bmatrix} \circ \begin{bmatrix} \mathbf{F}_{1,1} & \dots & \mathbf{F}_{1,N} \\ \vdots & \ddots & \vdots \\ \mathbf{F}_{N,1} & \dots & \mathbf{F}_{N,N} \end{bmatrix} \right) \mathbf{1}.$$

Matrix reformulation using Hadamard products

Hadamard product of two matrices $\mathbf{A} \circ \mathbf{B}$

$$\begin{bmatrix} \mathbf{A}_{11} & \dots & \mathbf{A}_{1n} \\ \vdots & \ddots & \vdots \\ \mathbf{A}_{n1} & \dots & \mathbf{A}_{nn} \end{bmatrix} \circ \begin{bmatrix} \mathbf{B}_{11} & \dots & \mathbf{B}_{1n} \\ \vdots & \ddots & \vdots \\ \mathbf{B}_{n1} & \dots & \mathbf{B}_{nn} \end{bmatrix} = \begin{bmatrix} \mathbf{A}_{11}\mathbf{B}_{11} & \dots & \mathbf{A}_{1n}\mathbf{B}_{1n} \\ \vdots & \ddots & \vdots \\ \mathbf{A}_{n1}\mathbf{B}_{n1} & \dots & \mathbf{A}_{nn}\mathbf{B}_{nn} \end{bmatrix}.$$

Rewrite an N-point (periodic) finite volume scheme as

$$\begin{bmatrix} \mathbf{F}_{1,2} - \mathbf{F}_{1,N} \\ \mathbf{F}_{2,3} - \mathbf{F}_{2,1} \\ \vdots \\ \mathbf{F}_{N,1} - \mathbf{F}_{N,N-1} \end{bmatrix} = \left(\underbrace{\begin{bmatrix} 0 & 1 & & -1 \\ -1 & 0 & 1 & \\ & \ddots & \ddots & 1 \\ 1 & & -1 & 0 \end{bmatrix}}_{\text{periodic central difference}} \circ \underbrace{\begin{bmatrix} \mathbf{F}_{1,1} & \dots & \mathbf{F}_{1,N} \\ \vdots & \ddots & \vdots \\ \mathbf{F}_{N,1} & \dots & \mathbf{F}_{N,N} \end{bmatrix}}_{\text{flux matrix } \mathbf{F}} \right) \mathbf{1}.$$

Matrix reformulation using Hadamard products

Hadamard product of two matrices $\mathbf{A} \circ \mathbf{B}$

$$\begin{bmatrix} \mathbf{A}_{11} & \dots & \mathbf{A}_{1n} \\ \vdots & \ddots & \vdots \\ \mathbf{A}_{n1} & \dots & \mathbf{A}_{nn} \end{bmatrix} \circ \begin{bmatrix} \mathbf{B}_{11} & \dots & \mathbf{B}_{1n} \\ \vdots & \ddots & \vdots \\ \mathbf{B}_{n1} & \dots & \mathbf{B}_{nn} \end{bmatrix} = \begin{bmatrix} \mathbf{A}_{11}\mathbf{B}_{11} & \dots & \mathbf{A}_{1n}\mathbf{B}_{1n} \\ \vdots & \ddots & \vdots \\ \mathbf{A}_{n1}\mathbf{B}_{n1} & \dots & \mathbf{A}_{nn}\mathbf{B}_{nn} \end{bmatrix}.$$

Rewrite an N-point (periodic) finite volume scheme as

$$\begin{bmatrix} \mathbf{F}_{1,2} - \mathbf{F}_{1,N} \\ \mathbf{F}_{2,3} - \mathbf{F}_{2,1} \\ \vdots \\ \mathbf{F}_{N,1} - \mathbf{F}_{N,N-1} \end{bmatrix} = 2(\mathbf{Q} \circ \mathbf{F})\mathbf{1}.$$

Interpretation using finite difference matrices

Let $\mathbf{M} = h\mathbf{I}$. Can reformulate entropy conservative finite volume as

$$\mathbf{M}\frac{\mathrm{d}\mathbf{u}}{\mathrm{d}t} + 2\left(\mathbf{Q} \circ \mathbf{F}\right)\mathbf{1} = \mathbf{0}, \qquad \mathbf{Q} = \frac{1}{2}\begin{bmatrix} 0 & 1 & & -1 \\ -1 & 0 & 1 & \\ & \ddots & \ddots & 1 \\ 1 & & -1 & 0 \end{bmatrix}$$

Note: $\mathbf{M}^{-1}\mathbf{Q}$ is a 2nd order (periodic) differentiation matrix.

Key result: generalizable beyond finite volumes

Entropy conservation for any $\underbrace{\mathbf{Q} = -\mathbf{Q}^T}_{\text{skew-symmetry}}$ and $\underbrace{\mathbf{Q1} = \mathbf{0}}_{\text{conservative}}$!

Interpretation using finite difference matrices

Let $\mathbf{M} = h\mathbf{I}$. Can reformulate entropy conservative finite volume as

$$\mathbf{M}\frac{\mathrm{d}\mathbf{u}}{\mathrm{dt}} + 2\left(\mathbf{Q} \circ \mathbf{F}\right)\mathbf{1} = \mathbf{0}, \qquad \mathbf{Q} = \frac{1}{2}\begin{bmatrix} 0 & 1 & & -1 \\ -1 & 0 & 1 & \\ & \ddots & \ddots & 1 \\ 1 & & -1 & 0 \end{bmatrix}$$

Note: $\mathbf{M}^{-1}\mathbf{Q}$ is a 2nd order (periodic) differentiation matrix.

Key result: generalizable beyond finite volumes

Entropy conservation for any $\underbrace{\mathbf{Q} = -\mathbf{Q}^T}_{\text{skew-symmetry}}$ and $\underbrace{\mathbf{Q1} = \mathbf{0}}_{\text{conservative}}$!

Discontinuous Galerkin spectral element methods (DGSEM)

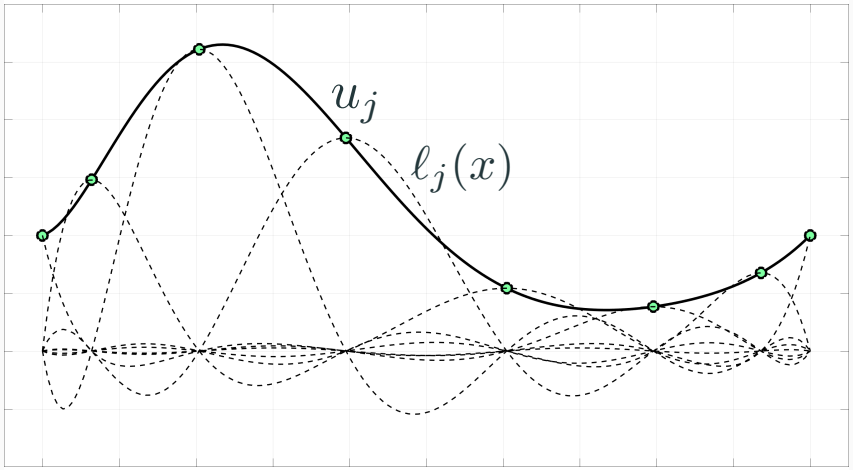

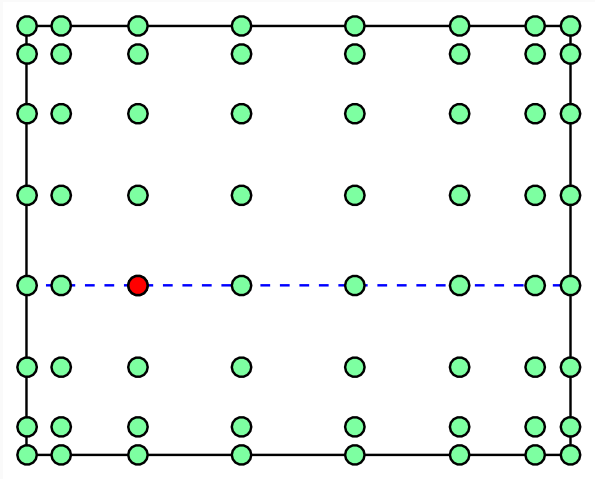

- Define weak differentiation matrix $\mathbf{Q}$, face extraction matrix $\mathbf{E}$

$$\mathbf{Q}_{ij} = \int_{-1}^{1} \frac{\partial \ell_j(x)}{\partial x} \ell_i(x), \qquad \mathbf{E} = \begin{bmatrix} 1 & 0 & \dots & 0 \\ 0 & \dots & 0 & 1 \end{bmatrix}.$$

- Can show $\mathbf{Q}$ is conservative and has the summation-by-parts (SBP) property under Lobatto quadrature.

$$\boxed{\mathbf{Q1} = \mathbf{0}, \qquad \mathbf{Q} + \mathbf{Q}^T = \mathbf{E}^T \mathbf{B} \mathbf{E}}, \qquad \mathbf{B} = \begin{bmatrix} -1 & 0 \\ 0 & 1 \end{bmatrix}.$$

Extension to multiple elements

- Let $\mathbf{M}$ be a diagonal mass matrix, $\mathbf{Q}$ be a conservative (e.g., $\mathbf{Q1} = \mathbf{0}$) SBP operator.

$$\mathbf{M}\frac{\mathrm{d}\mathbf{u}}{\mathrm{dt}} + 2\left(\mathbf{Q} \circ \mathbf{F}\right)\mathbf{1} + \mathbf{E}^T\mathbf{B}\Big(\underbrace{\boldsymbol{f}^*\left(\mathbf{u}^+, \mathbf{u}\right)}_{\text{interface flux}} - \boldsymbol{f}(\mathbf{u})\Big) = \mathbf{0}.$$

- Can prove that, for an entropy stable interface flux, the quadrature version of the local (cell) entropy inequality holds:

$$\int_{D^k} \frac{\partial S(\boldsymbol{u})}{\partial t} + \int_{\partial D^k} \left(\boldsymbol{v}^T \boldsymbol{f}^* - \psi\left(\boldsymbol{u}\right)\right) n \leq 0.$$

Fisher and Carpenter (2014), Gassner, Winters, and Kopriva (2016), Chen and Shu (2017), etc.

Extension to multiple elements

- Let $\mathbf{M}$ be a diagonal mass matrix, $\mathbf{Q}$ be a conservative (e.g., $\mathbf{Q1} = \mathbf{0}$) SBP operator.

$$\mathbf{M}\frac{\mathrm{d}\mathbf{u}}{\mathrm{dt}} + 2\left(\mathbf{Q} \circ \mathbf{F}\right)\mathbf{1} + \mathbf{E}^T\mathbf{B}\Big(\underbrace{\boldsymbol{f}^*\left(\mathbf{u}^+, \mathbf{u}\right)}_{\text{interface flux}} - \boldsymbol{f}(\mathbf{u})\Big) = \mathbf{0}.$$

- Can prove that, for an entropy stable interface flux, the quadrature version of the local (cell) entropy inequality holds:

$$\boxed{\int_{D^k} \frac{\partial S(\boldsymbol{u})}{\partial t} + \int_{\partial D^k} \left(\boldsymbol{v}^T \boldsymbol{f}^* - \psi\left(\boldsymbol{u}\right)\right) n \leq 0.}$$

Fisher and Carpenter (2014), Gassner, Winters, and Kopriva (2016), Chen and Shu (2017), etc.

Positivity preserving entropy stable nodal DG for the compressible Navier-Stokes equations (Yimin Lin)

Entropy stability requires positivity

Entropy stable schemes require positivity of density, pressure (numerical fluxes depend on *logarithm* of density, temperature).

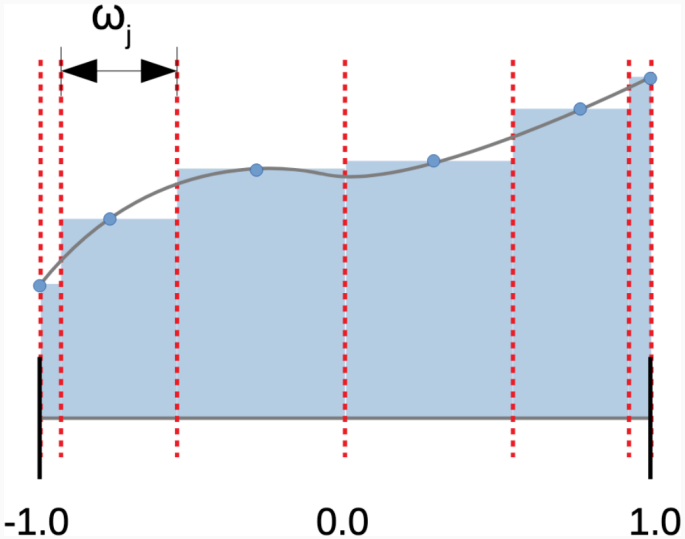

Interpretation of Lobotto nodes as a sub-cell finite volume grid.

- Hard to enforce both high order accuracy and positivity.
- Strategy: enforce positivity while retaining subcell resolution.

Rueda-Ramirez, Hennemann, Hindenlang, Winters, Gassner (2021). *An entropy stable nodal DG method for the resistive MHD equations. Part II: Subcell finite volume shock capturing*.

Enforcing positivity: a low order subcell scheme

Restricted to nodal methods (e.g., mass lumping, collocation).

Global formulation using forward Euler (higher order via SSP-RK).

Let $\mathbf{Q}_{ij} = -\mathbf{Q}_{ij}$, $\mathbf{f}_j = \boldsymbol{f}(\mathbf{u}_j)$, and $\mathbf{d}_{ij} = \mathbf{d}_{ji} > 0$

$$\mathbf{m}_i \frac{\mathbf{u}_i^{k+1} - \mathbf{u}_i}{\Delta t} + \sum_j \mathbf{Q}_{ij}\mathbf{f}_j - \underbrace{\mathbf{d}_{ij}\left(\mathbf{u}_j - \mathbf{u}_i\right)}_{\text{algebraic dissipation}} = \mathbf{0}.$$

Use conservation, SBP properties to rewrite using intermediate "bar states" $\bar{\mathbf{u}}_{ij} = \frac{1}{2}\left(\mathbf{u}_i + \mathbf{u}_j\right) - \frac{\mathbf{Q}_{ij}}{\mathbf{d}_{ij}}\left(\mathbf{f}_j - \mathbf{f}_i\right)$.

$$\frac{\mathbf{m}_i}{\Delta t}\mathbf{u}_i^{k+1} = \left(\frac{\mathbf{m}_i}{\Delta t} - \sum_{j \neq i} 2\mathbf{d}_{ij}\right)\mathbf{u}_i + \sum_{j \neq i} \frac{2\Delta t \mathbf{d}_{ij}}{\mathbf{m}_i}\bar{\mathbf{u}}_{ij}.$$

Guermond, Popov, and Tomas (2019). *Invariant domain preserving discretization-independent schemes and convex limiting for hyperbolic systems.*

Enforcing positivity: a low order subcell scheme

Restricted to nodal methods (e.g., mass lumping, collocation).

Global formulation using forward Euler (higher order via SSP-RK).

Let $\mathbf{Q}_{ij} = -\mathbf{Q}_{ij}$, $\mathbf{f}_j = \boldsymbol{f}(\mathbf{u}_j)$, and $\mathbf{d}_{ij} = \mathbf{d}_{ji} > 0$

$$\mathbf{m}_i \frac{\mathbf{u}_i^{k+1} - \mathbf{u}_i}{\Delta t} + \sum_j \mathbf{Q}_{ij}\mathbf{f}_j - \underbrace{\mathbf{d}_{ij}(\mathbf{u}_j - \mathbf{u}_i)}_{\text{algebraic dissipation}} = \mathbf{0}.$$

Use conservation, SBP properties to rewrite using intermediate "bar states" $\bar{\mathbf{u}}_{ij} = \frac{1}{2}(\mathbf{u}_i + \mathbf{u}_j) - \frac{\mathbf{Q}_{ij}}{\mathbf{d}_{ij}}(\mathbf{f}_j - \mathbf{f}_i)$.

$$\frac{\mathbf{m}_i}{\Delta t}\mathbf{u}_i^{k+1} = \left(\frac{\mathbf{m}_i}{\Delta t} - \sum_{j\neq i} 2\mathbf{d}_{ij}\right)\mathbf{u}_i + \sum_{j\neq i} \frac{2\Delta t \mathbf{d}_{ij}}{\mathbf{m}_i}\bar{\mathbf{u}}_{ij}.$$

Guermond, Popov, and Tomas (2019). *Invariant domain preserving discretization-independent schemes and convex limiting for hyperbolic systems.*

Enforcing positivity: a low order subcell scheme

Restricted to nodal methods (e.g., mass lumping, collocation).

Global formulation using forward Euler (higher order via SSP-RK).
Let $\mathbf{Q}_{ij} = -\mathbf{Q}_{ij}$, $\mathbf{f}_j = \boldsymbol{f}(\mathbf{u}_j)$, and $\mathbf{d}_{ij} = \mathbf{d}_{ji} > 0$

$$\mathbf{m}_i \frac{\mathbf{u}_i^{k+1} - \mathbf{u}_i}{\Delta t} + \sum_j \mathbf{Q}_{ij}\mathbf{f}_j - \underbrace{\mathbf{d}_{ij}\left(\mathbf{u}_j - \mathbf{u}_i\right)}_{\text{algebraic dissipation}} = \mathbf{0}.$$

Use conservation, SBP properties to rewrite using intermediate "bar states" $\bar{\mathbf{u}}_{ij} = \frac{1}{2}\left(\mathbf{u}_i + \mathbf{u}_j\right) - \frac{\mathbf{Q}_{ij}}{\mathbf{d}_{ij}}(\mathbf{f}_j - \mathbf{f}_i)$.

$$\frac{\mathbf{m}_i}{\Delta t}\mathbf{u}_i^{k+1} = \left(\frac{\mathbf{m}_i}{\Delta t} - \sum_{j\neq i} 2\mathbf{d}_{ij}\right)\mathbf{u}_i + \sum_{j\neq i} \frac{2\Delta t \mathbf{d}_{ij}}{\mathbf{m}_i}\bar{\mathbf{u}}_{ij}.$$

Guermond, Popov, and Tomas (2019). *Invariant domain preserving discretization-independent schemes and convex limiting for hyperbolic systems.*

Provable positivity under a CFL condition

- Bar states $\bar{\mathbf{u}}_{ij}$ preserve positivity for $\mathbf{d}_{ij}$ sufficiently large

$$\bar{\mathbf{u}}_{ij} = \frac{1}{2}\left(\mathbf{u}_i + \mathbf{u}_j\right) - \frac{\mathbf{Q}_{ij}}{\mathbf{d}_{ij}}\left(\mathbf{f}_j - \mathbf{f}_i\right), \qquad \mathbf{d}_{ij} \geq \lambda_{\max}\left(\mathbf{u}_i, \mathbf{u}_j, \mathbf{Q}_{ij}\right).$$

- $\mathbf{u}_i^{k+1}$ is positive (e.g., convex combination of $\mathbf{u}_i$ and $\bar{\mathbf{u}}_{ij}$) if

$$\Delta t \leq \min_i \frac{\mathbf{m}_i}{2\sum_{i \neq j} \mathbf{d}_{ij}}.$$

Guermond and Popov (2016). *Invariant domains and first-order continuous finite element approximation for hyperbolic systems.*

Our work: extension to compressible Navier-Stokes

- Entropy stable low order discretization of first order form of viscous terms $\boldsymbol{\sigma}$ = stress $\boldsymbol{\tau}$ + heat conduction $\boldsymbol{q}$.

$$\mathbf{M}\frac{\mathrm{d}\mathbf{u}}{\mathrm{dt}} + \sum_j \mathbf{Q}_{ij}\left(\mathbf{f}_j - \boldsymbol{\sigma}_j\right) - \mathbf{d}_{ij}\left(\mathbf{u}_j - \mathbf{u}_i\right) = \mathbf{0}.$$

- Reformulate scheme in terms of viscous bar states:

$$\bar{\mathbf{u}}_{ij} = \frac{1}{2}\left(\mathbf{u}_i + \mathbf{u}_j\right) - \frac{\mathbf{Q}_{ij}}{\mathbf{d}_{ij}}\left(\left(\mathbf{f}_j - \boldsymbol{\sigma}_j\right) - \left(\mathbf{f}_i - \boldsymbol{\sigma}_i\right)\right)$$

- Positivity of ρ, p under a (viscous) CFL condition with

$$\mathbf{d}_{ij} = \max\left(\beta(\mathbf{u}_i), \beta(\mathbf{u}_j), \lambda_{\max}(\mathbf{u}_i, \mathbf{u}_j, \mathbf{Q}_{ij}), \lambda_{\max}(\mathbf{u}_j, \mathbf{u}_i, \mathbf{Q}_{ji})\right)$$

$$\beta(\boldsymbol{u}) > |\boldsymbol{v}\cdot\boldsymbol{n}| + \frac{1}{2\rho^2 e}\left(\sqrt{\rho^2(\boldsymbol{q}\cdot\boldsymbol{n})^2 + 2\rho^2 e\,\|\boldsymbol{\tau}\cdot\boldsymbol{n} - p\boldsymbol{n}\|}\right) + \rho\,|\boldsymbol{q}\cdot\boldsymbol{n}|$$

Chan, Lin, Warburton (2021). *Entropy stable modal dG schemes and wall BCs for the CNS equations*.

Zhang (2017). *On positivity-preserving high order DG schemes for the compressible NS equations*.

Sparsification of low order matrices

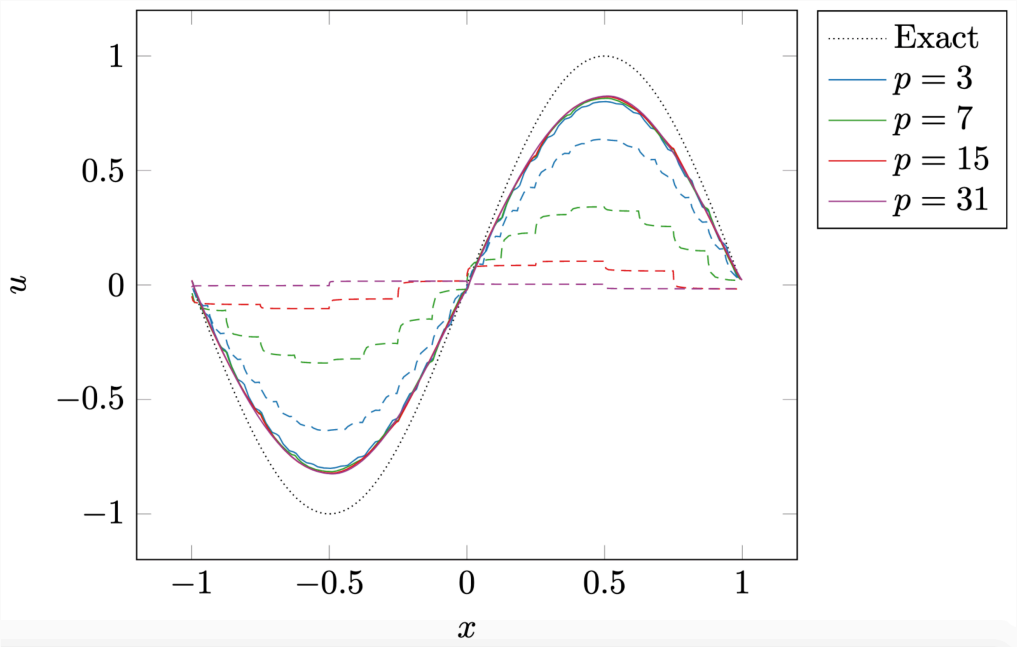

Effect of sparsification on solution dissipation; figure taken from Pazner (2021).

- Algebraic artificial dissipation depends on discretization matrices $\Longrightarrow$ dense operators produce too much diffusion!
- New sparsified operators on simplicial elements inspired by the construction of meshfree methods.

Pazner (2021). *Sparse invariant domain preserving DG methods with subcell convex limiting*.

Trask, Bochev, Perugo (2020). *A conservative, consistent, and scalable meshfree mimetic method*.

Sparsification of low order matrices

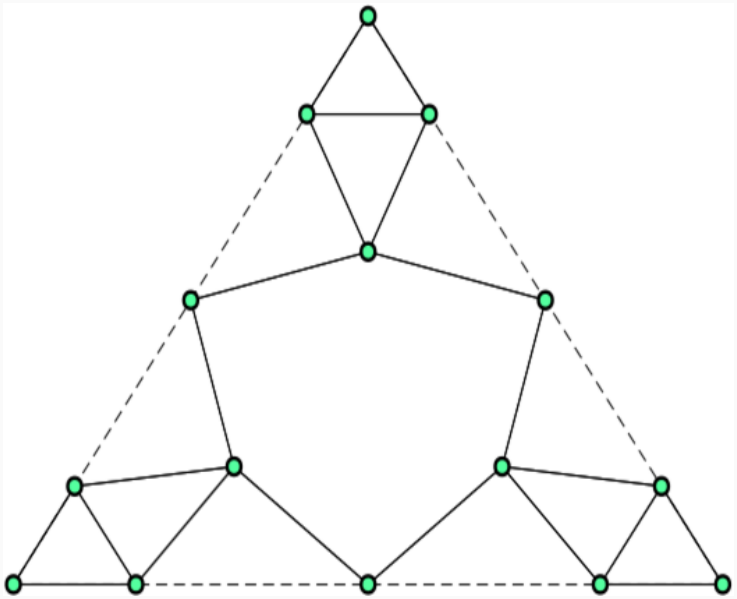

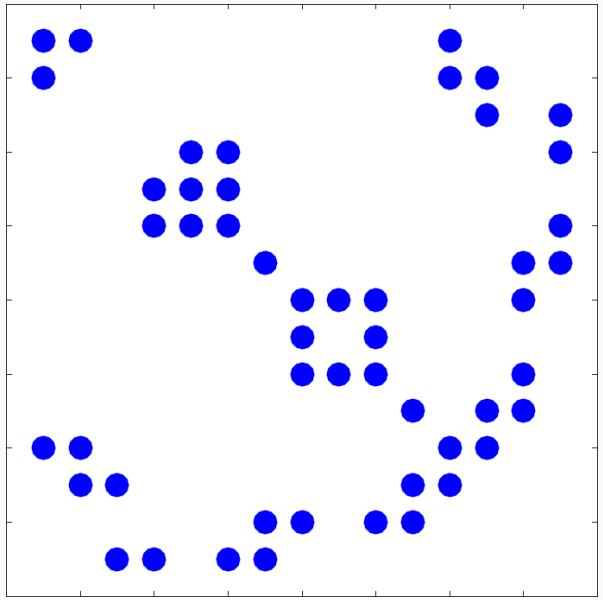

- Algebraic artificial dissipation depends on discretization matrices $\Longrightarrow$ dense operators produce too much diffusion!
- New sparsified operators on simplicial elements inspired by the construction of meshfree methods.

Pazner (2021). *Sparse invariant domain preserving DG methods with subcell convex limiting*.

Trask, Bochev, Perugo (2020). *A conservative, consistent, and scalable meshfree mimetic method*.

Sparse low order approximations to simplicial SBP operators

- Want to preserve conservation $\mathbf{Q}^{\text{low}}\mathbf{1} = \mathbf{0}$ and SBP property

$$\mathbf{Q}^{\text{low}} + \left(\mathbf{Q}^{\text{low}}\right)^T = \mathbf{B}.$$

- For neighboring i and j, assume

$$\left(\mathbf{Q}^{\text{low}} - \left(\mathbf{Q}^{\text{low}}\right)^T\right)_{ij} = \psi_j - \psi_i.$$

- Enforcing $\mathbf{Q}^{\text{low}}\mathbf{1} = \mathbf{0}$ equivalent to

$$\sum_j \psi_j - \psi_i = \left(-\frac{1}{2}\mathbf{B}\mathbf{1}\right)_i,$$

$$\text{s.t. } \boldsymbol{\psi}^T\mathbf{1} = 0.$$

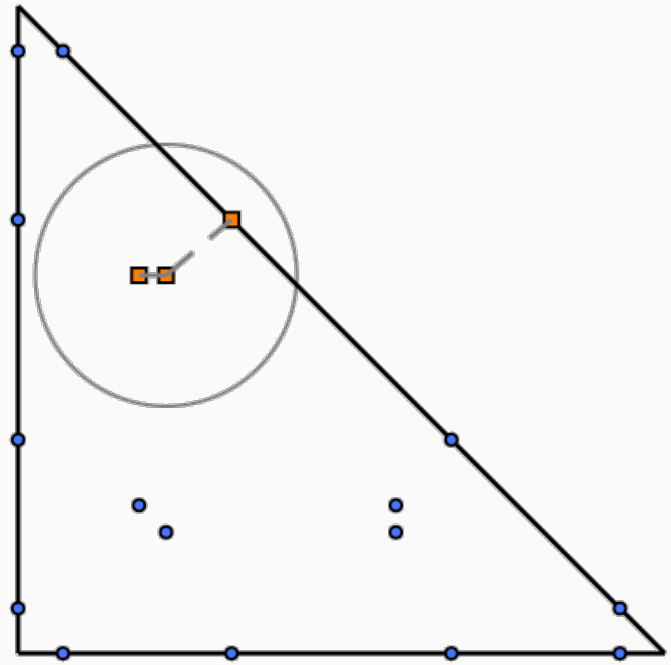

Quadrature nodes from Chen, Shu (2017) for a degree $N = 3$ SBP operator. The sparse low order operator $\mathbf{Q}^{\text{low}}$ uses the same nodes and weights.

Blending high and low order DG solutions

- Blend high and low order solutions over each element to retain accuracy where possible while ensuring positivity.

$$\mathbf{u}^{k+1} = (1-\ell)\mathbf{u}^{k+1,\text{low}} + \ell\mathbf{u}^{k+1,\text{high}}$$

- Impose minimal local bounds based on low order solution with relaxation factor α

$$\rho \geq \alpha\rho^{\text{low}}, \qquad p \geq \alpha p^{\text{low}}, \qquad \alpha \in [0,1].$$

- Local entropy inequality: preserved for element-wise blending.
- Local conservation: preserved if high and low order schemes use the same interface flux.

Convergence tests: LeBlanc and viscous shock tube

	$N = 2$		$N = 5$	
h	L^1 error	Rate	L^1 error	Rate
0.02	8.681×10^{-2}		5.956×10^{-2}	.
0.01	3.658×10^{-2}	1.25	1.436×10^{-2}	2.05
0.005	1.329×10^{-2}	1.46	3.630×10^{-3}	1.98
0.0025	6.015×10^{-3}	1.14	1.129×10^{-3}	1.69
0.00125	2.910×10^{-3}	1.05	5.889×10^{-4}	0.94

(a) Leblanc shock tube, relaxation factor $\alpha = 0.5$

	$N = 2$		$N = 3$	
h	L^1 error	Rate	L^1 error	Rate
0.025	2.305×10^{-2}		2.071×10^{-2}	
0.0125	9.858×10^{-2}	1.23	6.749×10^{-3}	1.62
0.00625	3.382×10^{-3}	1.54	1.278×10^{-3}	2.40
0.003125	5.765×10^{-4}	2.55	1.163×10^{-4}	3.45
0.0015625	8.836×10^{-5}	2.71	1.269×10^{-5}	3.20

(b) 1D viscous shock, $\mathrm{Re} = 1000$, relaxation factor $\alpha = 0.5$

Viscous shock is run at Mach 20 to generate positivity violations.

Isentropic vortex with small minimum density

	$N = 2$		$N = 3$		$N = 4$	
h	L^2 error	Rate	L^2 error	Rate	L^2 error	Rate
2.5	1.148×10^{0}		5.958×10^{-1}	1.28	4.073×10^{-1}	
1.25	4.865×10^{-1}	1.24	1.905×10^{-1}	1.64	8.987×10^{-2}	2.18
0.625	1.223×10^{-1}	1.99	2.308×10^{-2}	3.05	1.511×10^{-2}	2.57
0.3125	1.706×10^{-2}	2.84	2.393×10^{-3}	3.27	1.915×10^{-4}	6.30

(c) Quadrilateral meshes, relaxation factor $\alpha = 0.5$

	$N = 2$		$N = 3$		$N = 4$	
h	L^2 error	Rate	L^2 error	Rate	L^2 error	Rate
2.5	7.887×10^{-1}		5.034×10^{-1}		4.059×10^{-1}	
1.25	3.834×10^{-1}	1.04	1.881×10^{-1}	1.42	9.890×10^{-2}	2.04
0.625	8.993×10^{-2}	2.09	2.944×10^{-2}	2.68	1.578×10^{-2}	2.65
0.3125	1.298×10^{-2}	2.79	2.606×10^{-3}	3.50	4.258×10^{-4}	5.21

(d) Triangular meshes, relaxation factor $\alpha = 0.5$

Challenging vortex parameters: $\rho_{\min} = 2.145 \times 10^{-3}$!

Compressible Euler: double Mach reflection

(a) Subcell positivity-preserving entropy stable nodal DG, $\alpha = 0.5$, $T = .2$

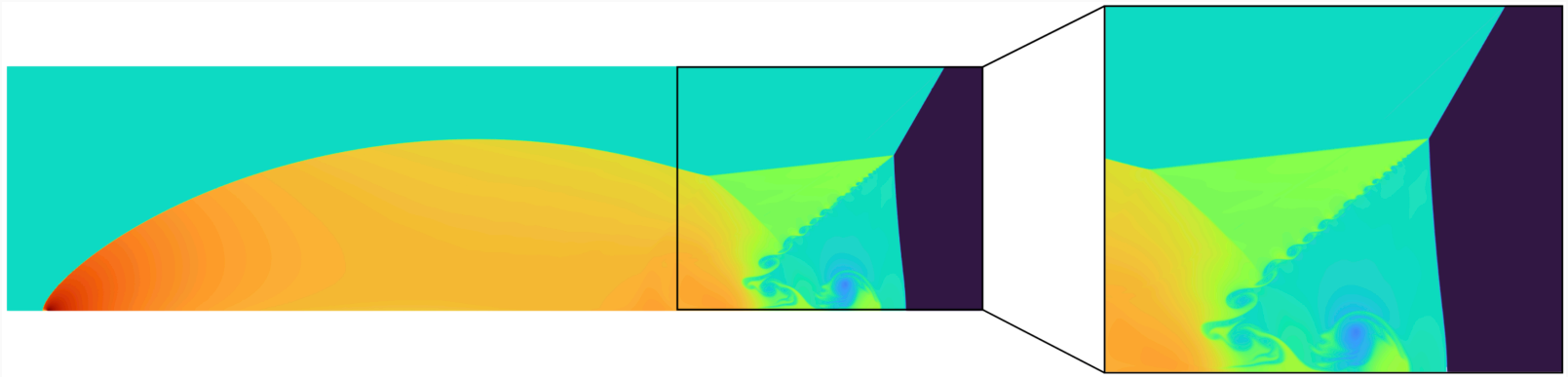

(b) Subcell invariant domain preserving nodal DG (Pazner 2021), $T = .275$

Density for $N = 3$ entropy stable DG (250×875 elements) and a reference solution (600×2400 elements). Note: positivity is sensitive to the wall boundary treatment!

---

van der Vegt and Ven (2002). *Slip flow boundary conditions in dG discretizations of the Euler equations [...].*

Compressible Euler: Sedov blast wave

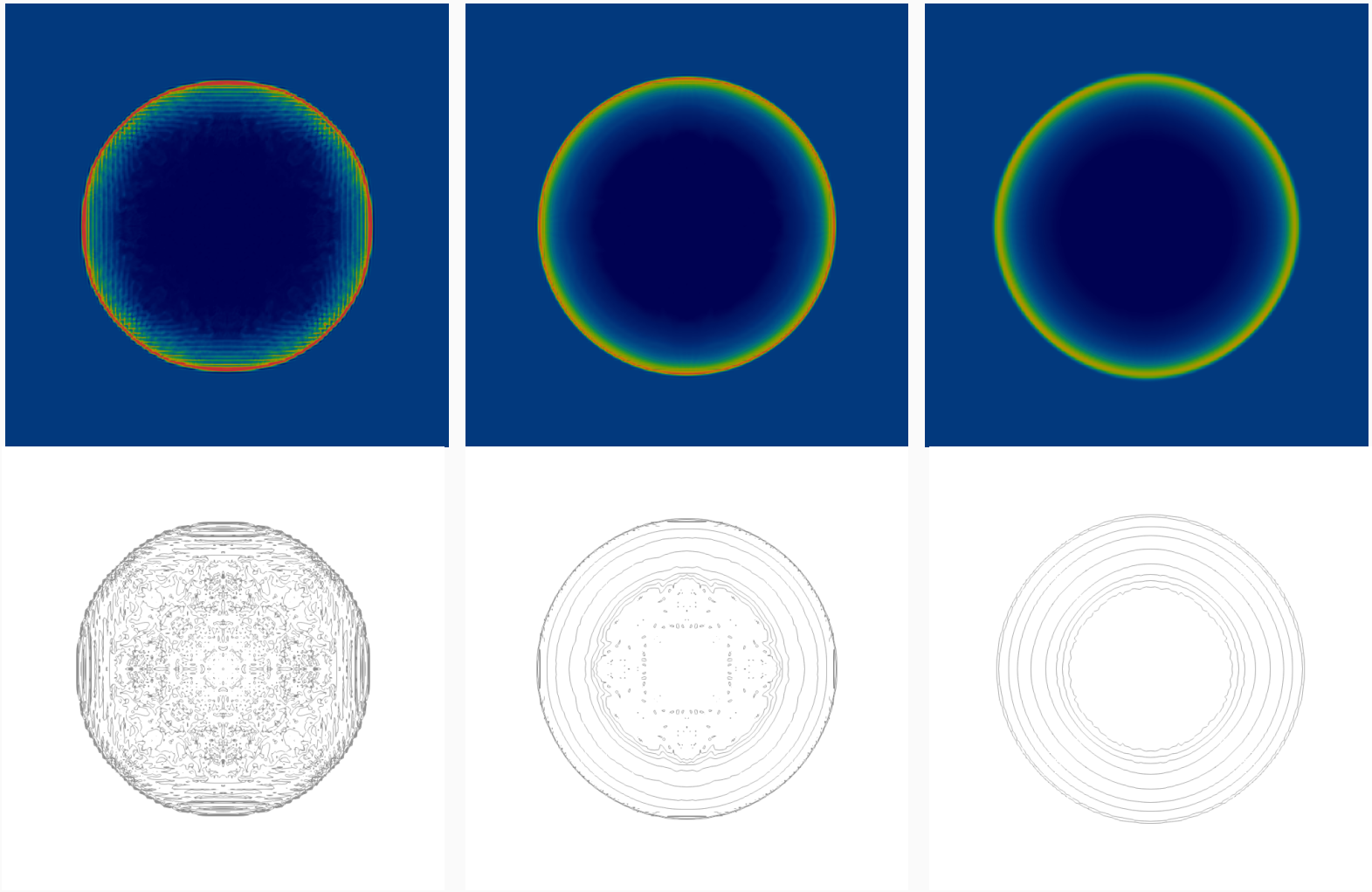

(a) $\alpha = 0.1$ **(b)** $\alpha = 0.5$ **(c)** $\alpha = 0.1$ + shock capturing

Quadrilateral meshes with 100^2 degree $N = 3$ elements.

Compressible Euler: Sedov blast wave

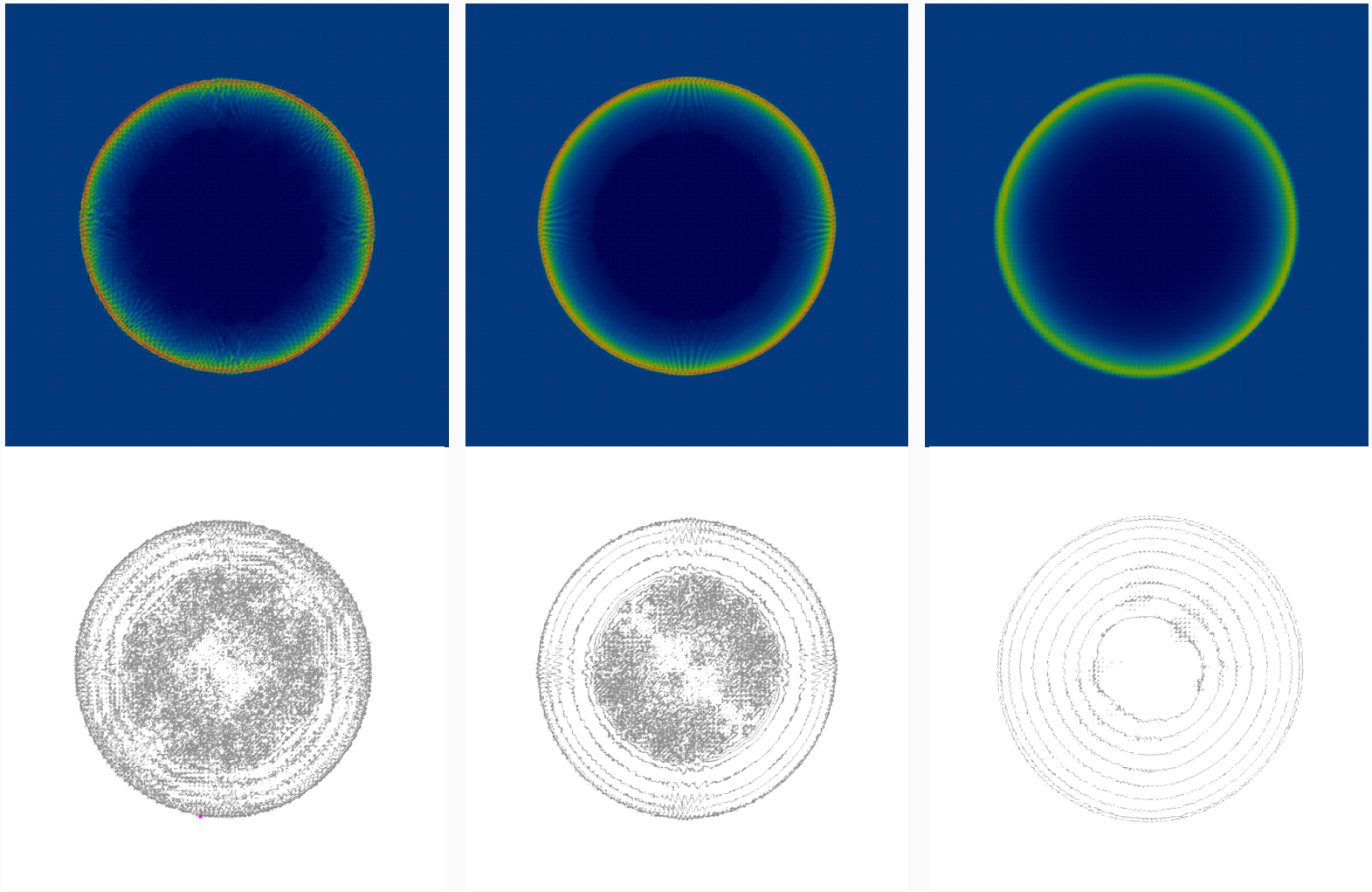

(a) $\alpha = 0.1$ **(b)** $\alpha = 0.5$ **(c)** $\alpha = 0.1$ + shock capturing

Triangular meshes with 100^2 degree $N = 3$ elements.

Compressible Navier-Stokes: Daru-Tenaud shock tube

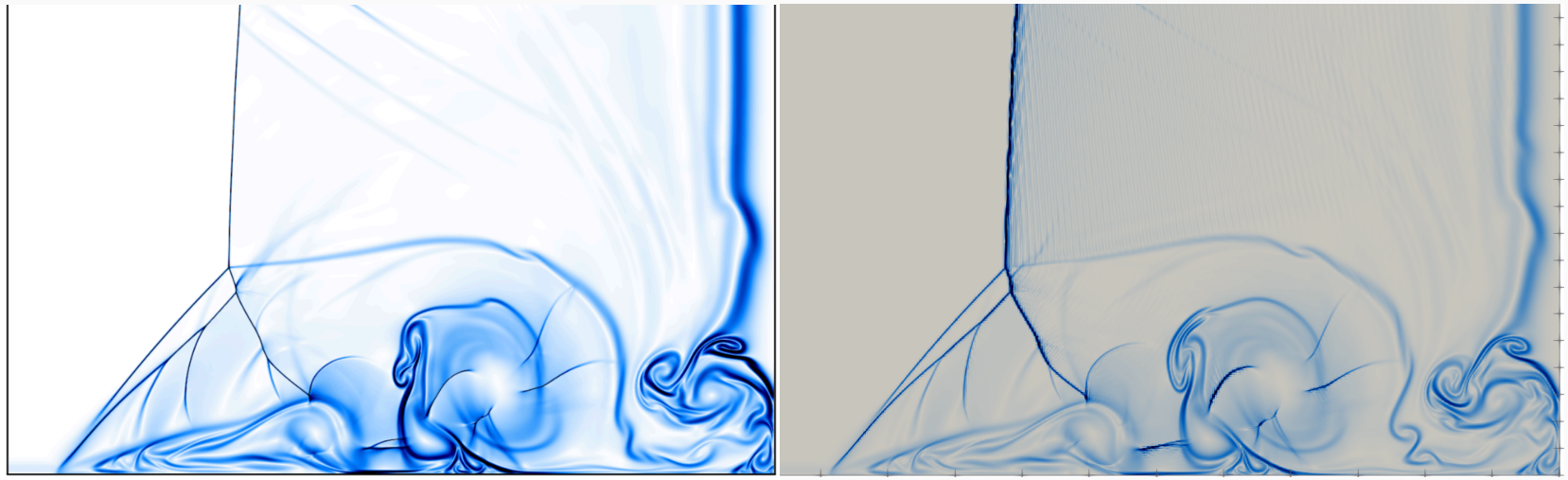

(a) Reference solution (512M nodes) **(b)** Degree $N = 3$, 600×300 grid

Comparison with a "grid-converged" reference solution from Guermond et al. (2022).

Guermond, Kronbichler, Maier, Popov, Tomas (2022). *On the implementation of a robust and efficient finite element-based parallel solver for the compressible Navier-Stokes equations.*

Sensitivity to polynomial degree and mesh size

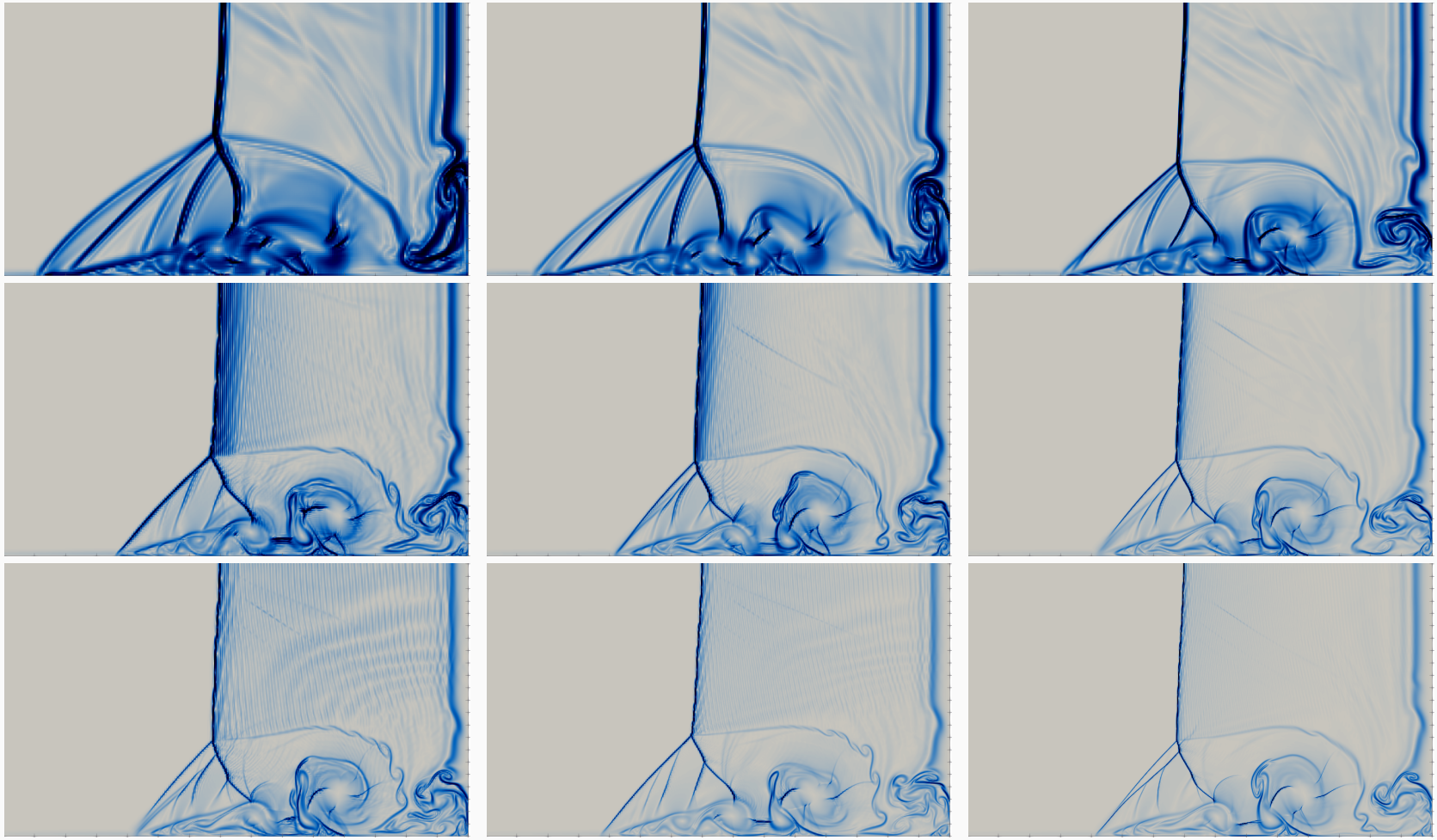

Polynomial degrees $N = 1, 2, 3$ (rows) and $300 \times 150, 400 \times 200, 600 \times 300$ grid resolutions (columns). The limiting relaxation factor is $\alpha = 0.1$.

Daru, Tenaud (2009). *Numerical simulation of the viscous shock tube problem by using a high resolution monotonicity-preserving scheme*.

Sensitivity to shock capturing and artificial viscosity

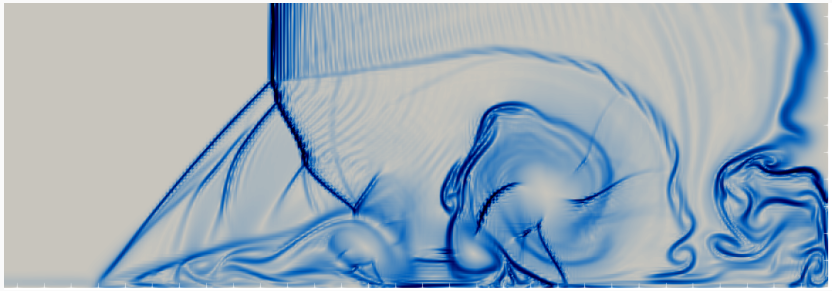

(a) $\alpha = 0.1$ ($N = 2$, 400×200 grid)

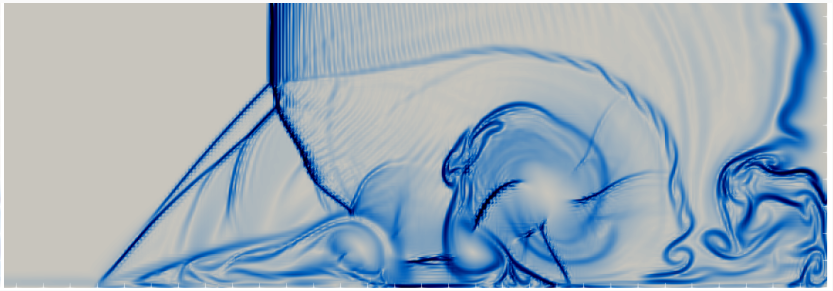

(b) $\alpha = 0.5$ ($N = 2$, 400×200 grid)

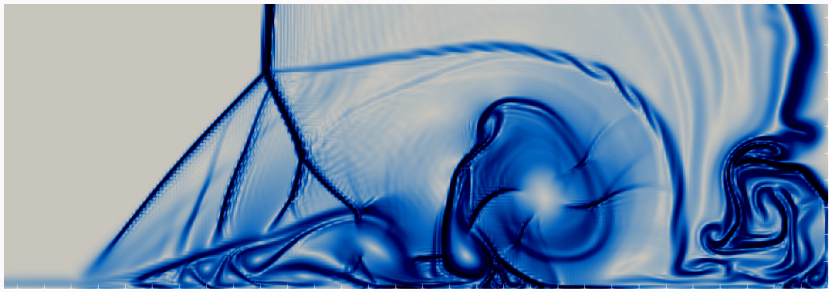

(c) $\alpha = 0.1$ + shock capturing ($N = 2$, 400×200 grid)

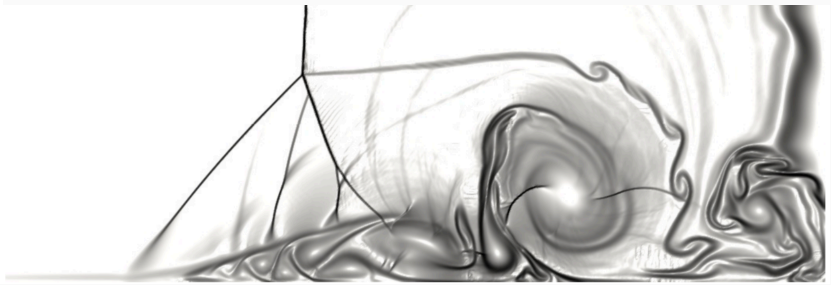

(d) Dzanic, Witherden ($N = 4$, 800×400 grid)

For degree $N = 2$ on a 400×200 grid, the solution is sensitive to additional shock capturing but less sensitive to limiting parameters.

Dzanic, Witherden (2022). *Positivity-Preserving Entropy-Based Adaptive Filtering for Discontinuous Spectral Element Methods.*

"Modal" entropy stable DG formulations

Beyond nodal formulations: entropy projection

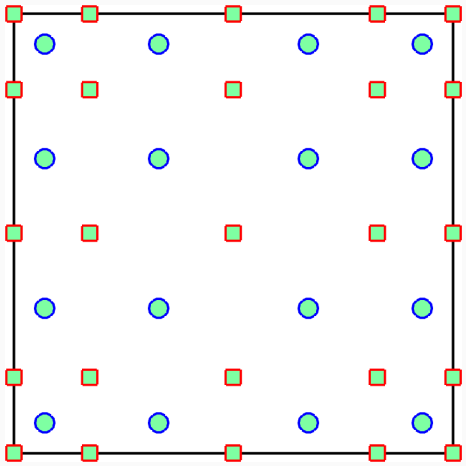

For non-collocated methods (e.g., staggered grid, modal), entropy stability requires interpolating using the "entropy projection"

$$\widetilde{\boldsymbol{u}} = \boldsymbol{u}\left(\Pi_N \boldsymbol{v}(\boldsymbol{u})\right)$$

$\Pi_N = L^2$ projection onto degree N polynomials.

- Entropy projection recovers nodal collocation for appropriate choices of quadrature for the L^2 projection.
- Entropy stable modal formulations also require boundary correction terms for high order accuracy (Chan 2018, 2019).

Parsani, Carpenter, Fisher, Nielsen (2016). *Entropy stable staggered grid discontinuous spectral collocation methods of any order for the compressible Navier-Stokes equations*.

Fernandez, Crean, Carpenter, Hicken (2019). *Staggered-grid entropy-stable multidimensional summation-by-parts discretizations on curvilinear coordinates*.

Pazner, Persson (2019). *Analysis and entropy stability of the line-based discontinuous Galerkin method*.

Illustration of the entropy projection

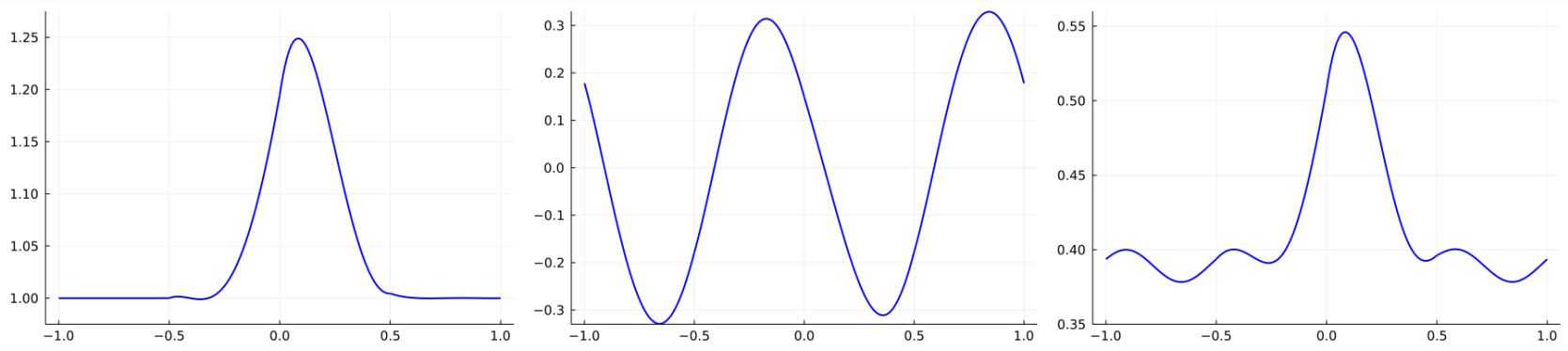

(a) ρ **(b)** u **(c)** p

Primitive variables ρ, u, p and their entropy projection.

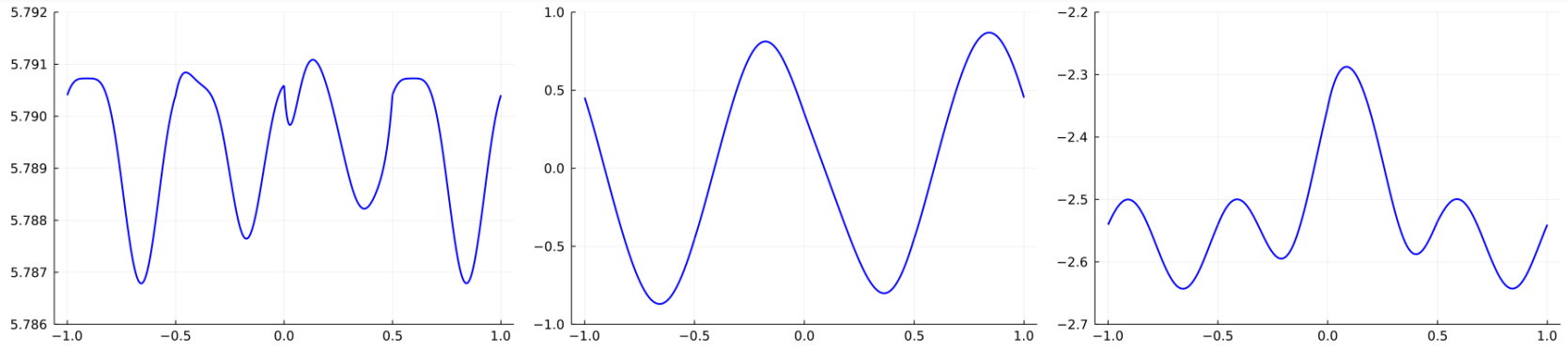

(d) v_1 **(e)** v_2 **(f)** v_3

Entropy variables and their L^2 projection.

Illustration of the entropy projection

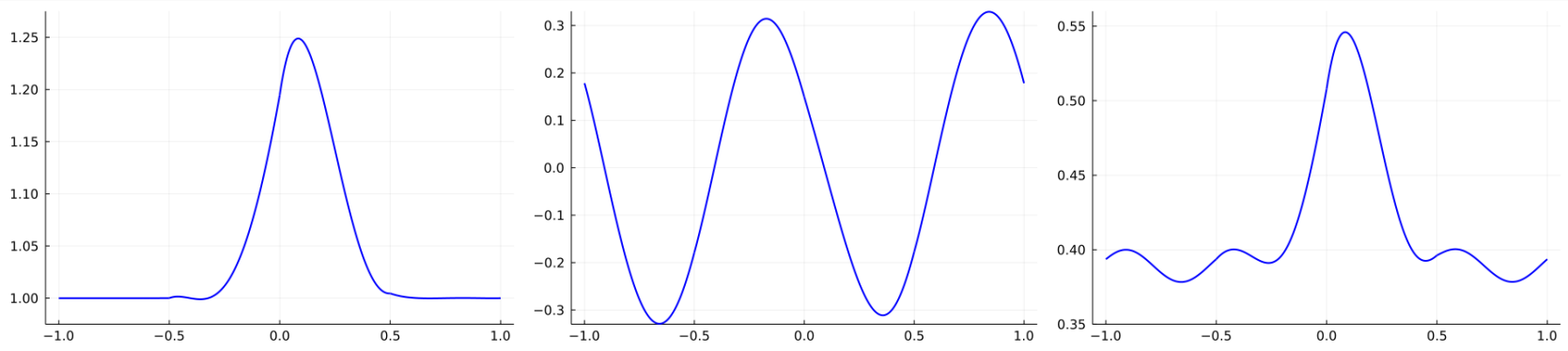

(a) ρ **(b)** u **(c)** p

Primitive variables ρ, u, p and their entropy projection.

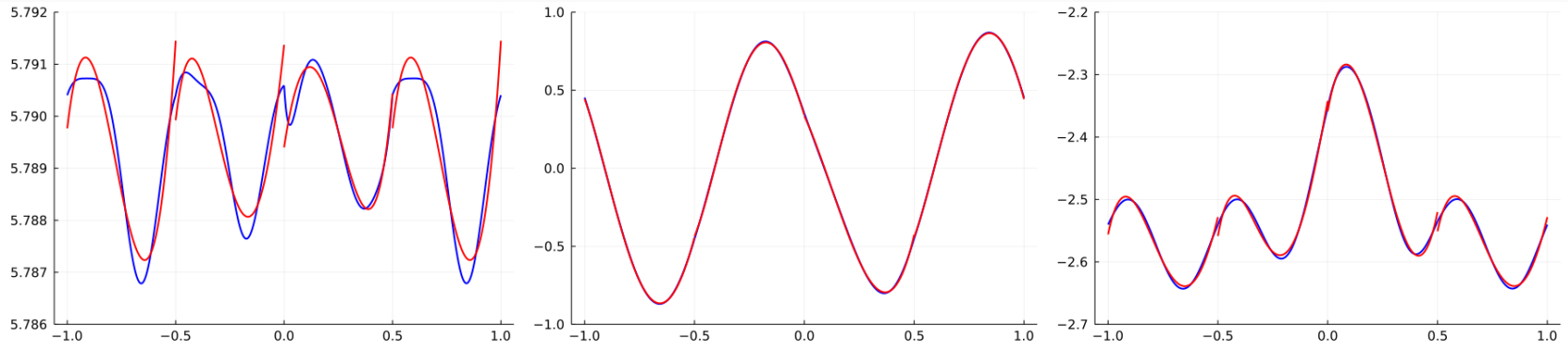

(d) v_1 **(e)** v_2 **(f)** v_3

Entropy variables and their L^2 projection.

Illustration of the entropy projection

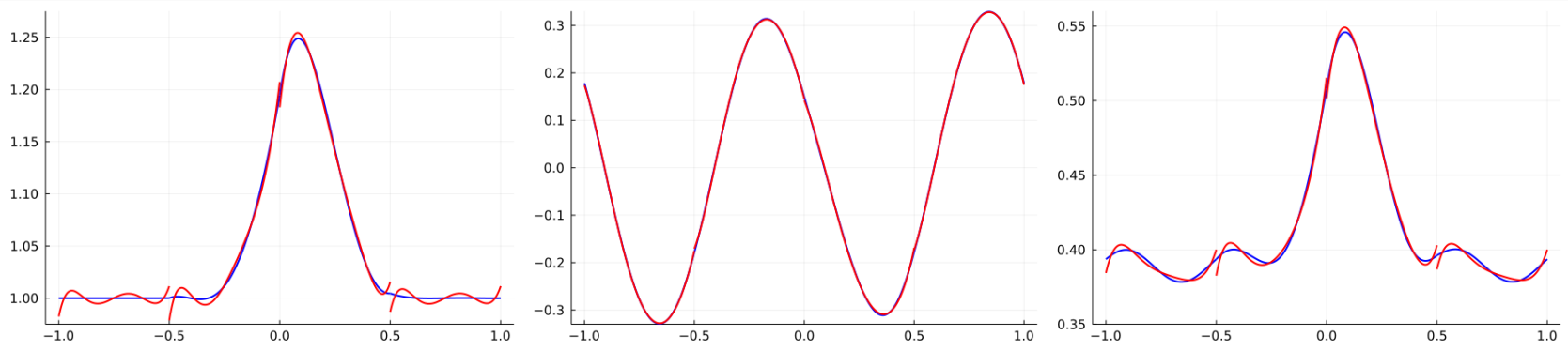

(a) ρ **(b)** u **(c)** p

Primitive variables ρ, u, p and their entropy projection.

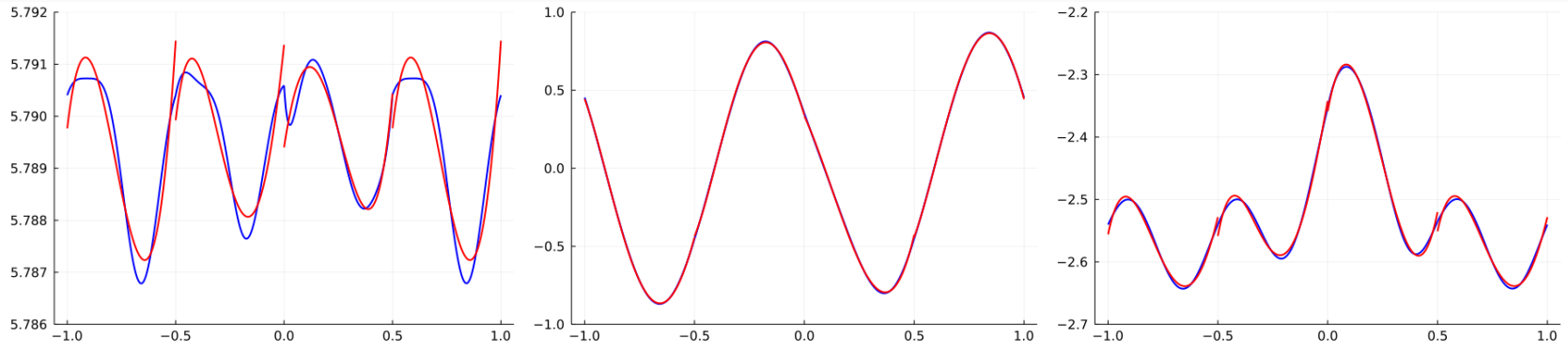

(d) v_1 **(e)** v_2 **(f)** v_3

Entropy variables and their L^2 projection.

Why "modal" formulations?

Nodal formulations: collocation, specific nodes and basis.

"Modal" formulations: arbitrary basis functions and quadrature.

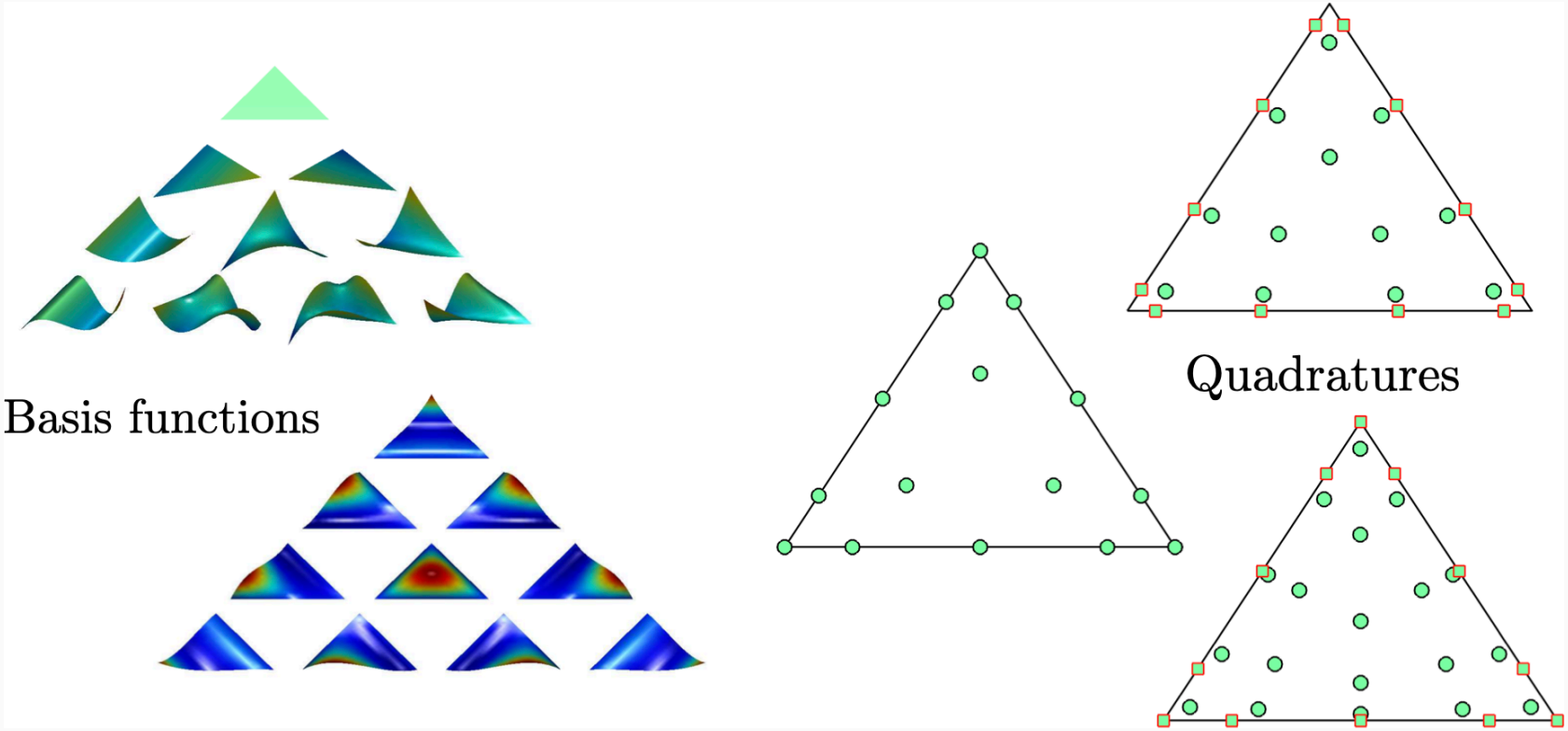

Enables standard finite element tools, recovers existing schemes.

Figures from http://www2.compute.dtu.dk/ apek/DGFEMCourse2009/Lecture05.pdf.

Why "modal" formulations?

Nodal formulations: collocation, specific nodes and basis.

"Modal" formulations: arbitrary basis functions and quadrature.

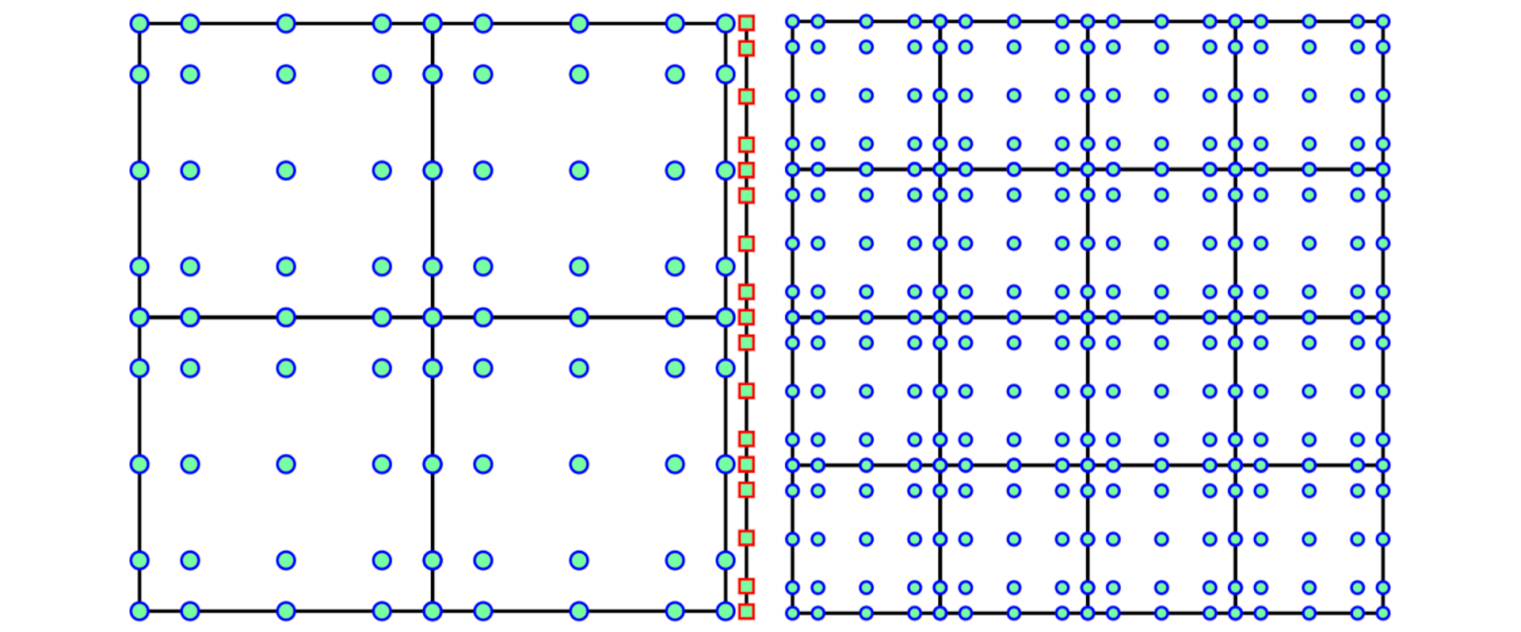

Modal formulations make non-conforming meshes simpler.

Chan, Bencomo, Del Rey Fernandez (2020). *Mortar-based entropy-stable discontinuous Galerkin methods on non-conforming quadrilateral and hexahedral meshes*.

Why "modal" formulations?

Nodal formulations: collocation, specific nodes and basis.

"Modal" formulations: arbitrary basis functions and quadrature.

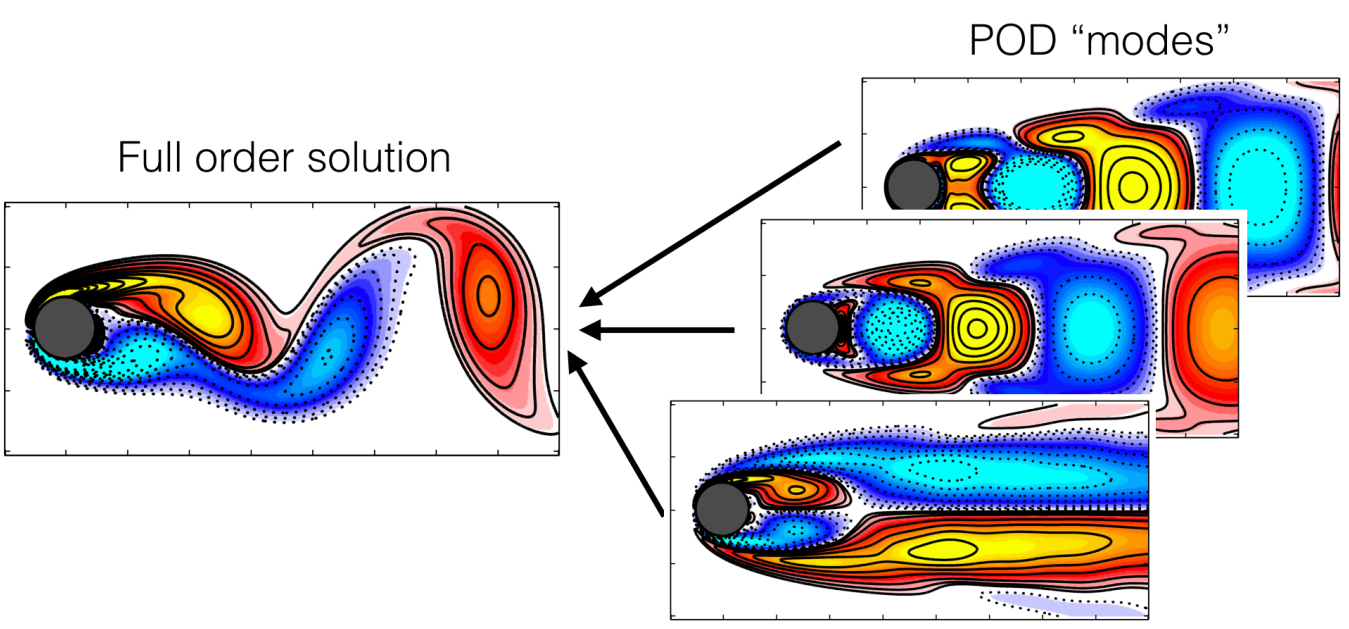

Projection-based reduced order models: learn basis functions from data.

Figure adapted from Brunton, Proctor, Kutz (2016), *Discovering governing equations from data . . . .*

Chan (2020). *Entropy stable reduced order modeling of nonlinear conservation laws.*

Chan, Bencomo, Del Rey Fernandez (2020). *Mortar-based entropy-stable discontinuous Galerkin methods on non-conforming quadrilateral and hexahedral meshes.*

Building on modal entropy stable formulations

Over the last few years:

- Entropy stable reduced order modeling
- Non-conforming meshes (Mario Bencomo, DCDR Fernandez)
- Networks and multi-dimensional domains (Philip Wu)
- Quasi-1D equations (Charlie Liu, Philip Wu, and more)
- Entropy stable formulations and boundary conditions for compressible Navier-Stokes (Yimin Lin, T. Warburton)
- Robust high order DG for under-resolved flows
- Positivity-preserving methods for modal entropy stable schemes (in progress).

Modal ESDG: compressible Navier-Stokes flow over a square

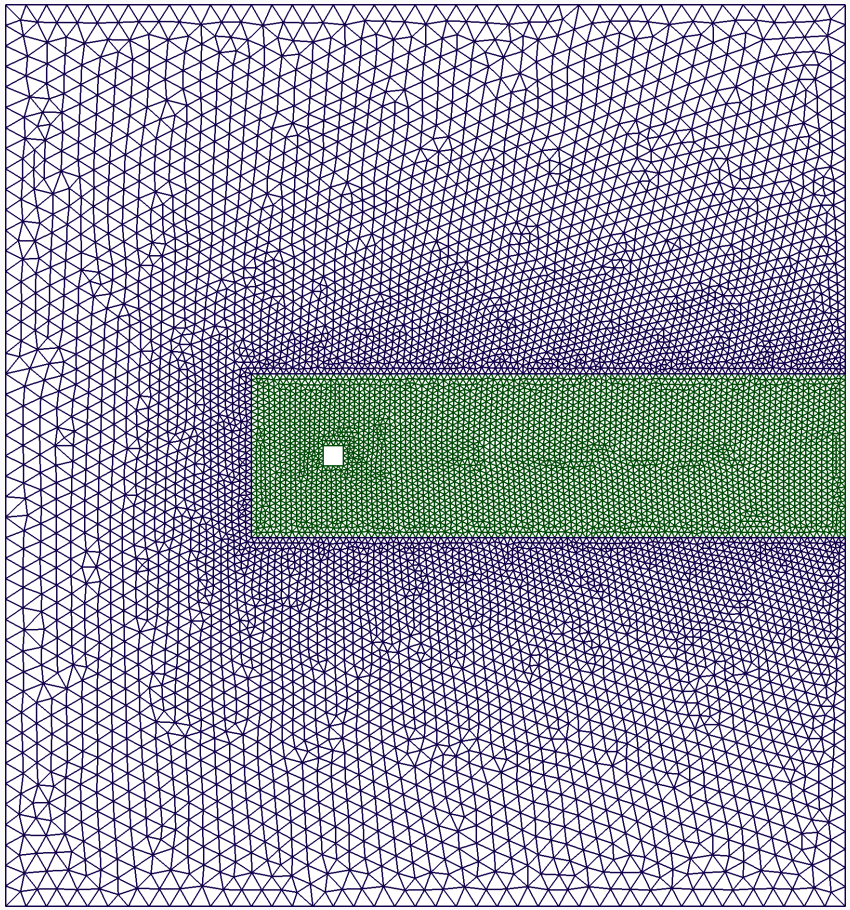

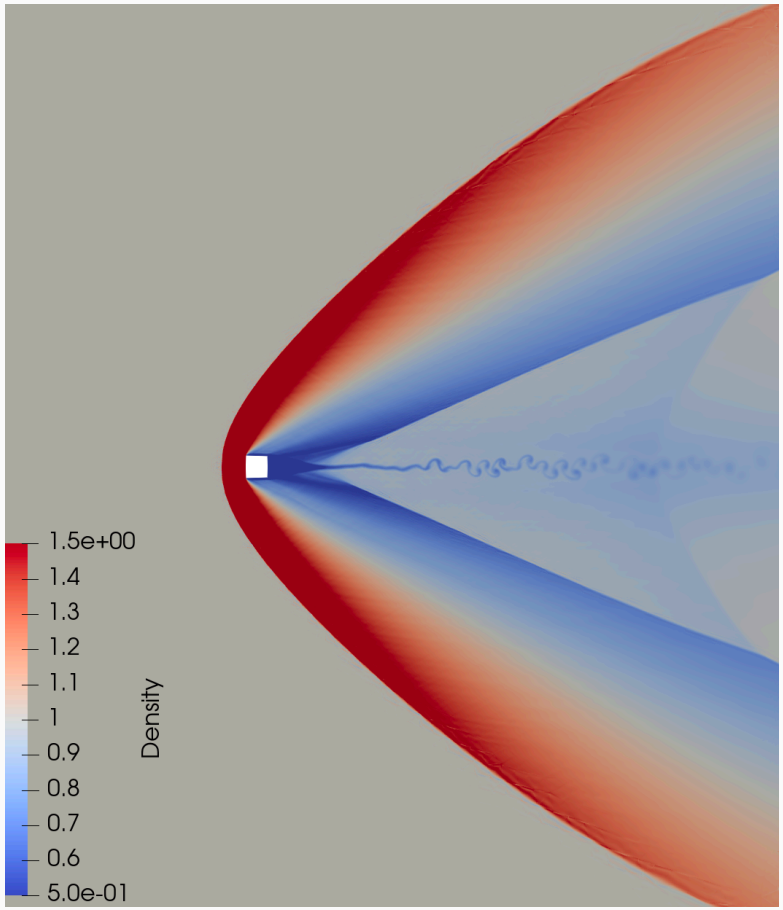

Density at $T_{\text{final}} = 100$ for $\text{Re} = 10^4, \text{Ma} = 1.5$ for a degree $N = 3$ mesh with $16,574$ elements. Discretization of diffusive terms: symmetrization of viscous fluxes, stable imposition of wall boundary conditions.

"Modal" entropy stable DG formulations

Differences in robustness for different entropy stable schemes

This section uses the Julia library Trixi.jl, adaptive explicit RK

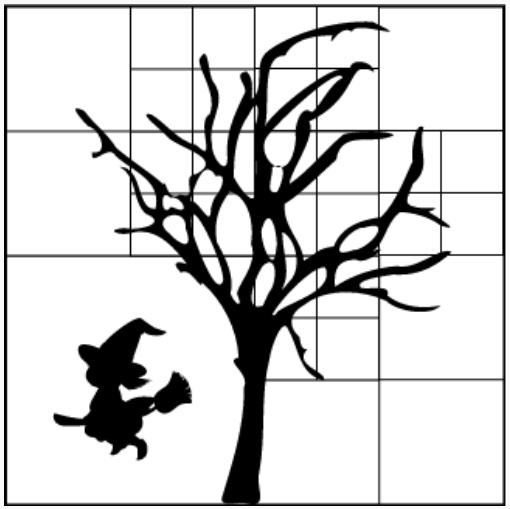

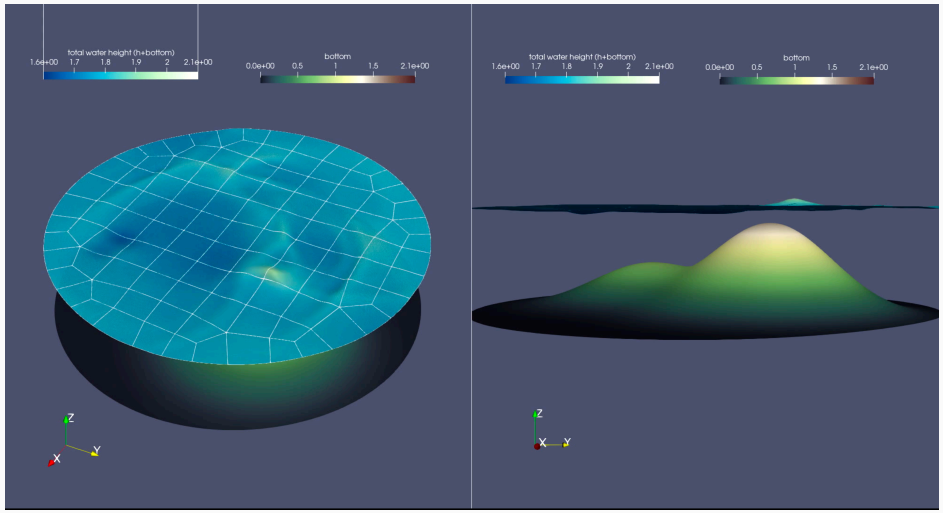

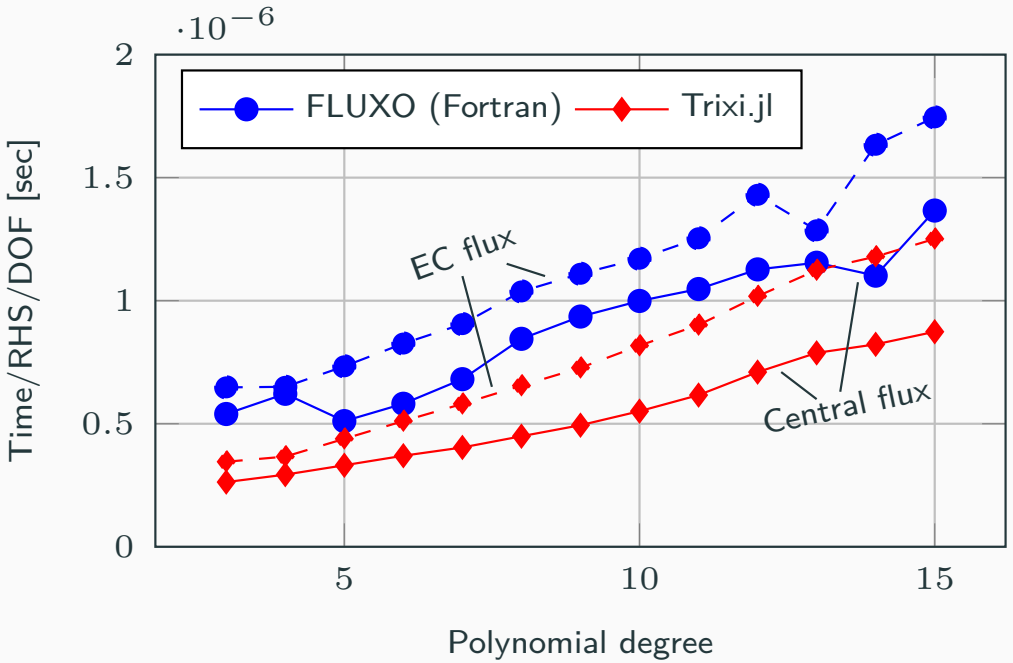

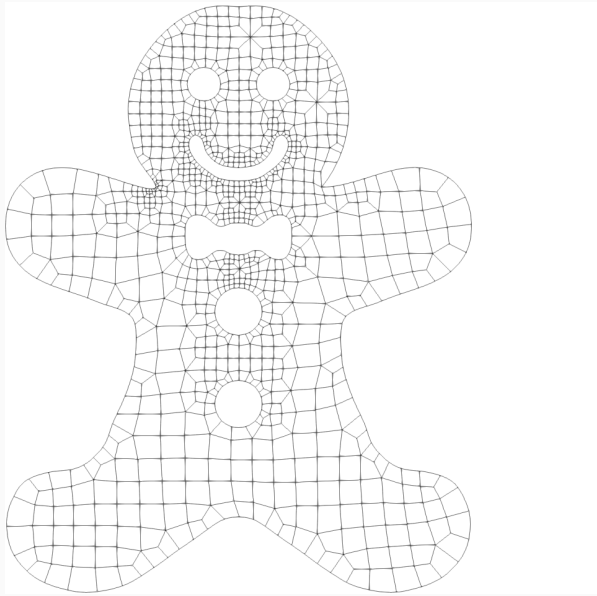

Ranocha, et al. (2021). *Optimized RK Methods with Auto. Step Size Control for Compressible CFD.*

Differences in ESDG robustness for compressible Euler

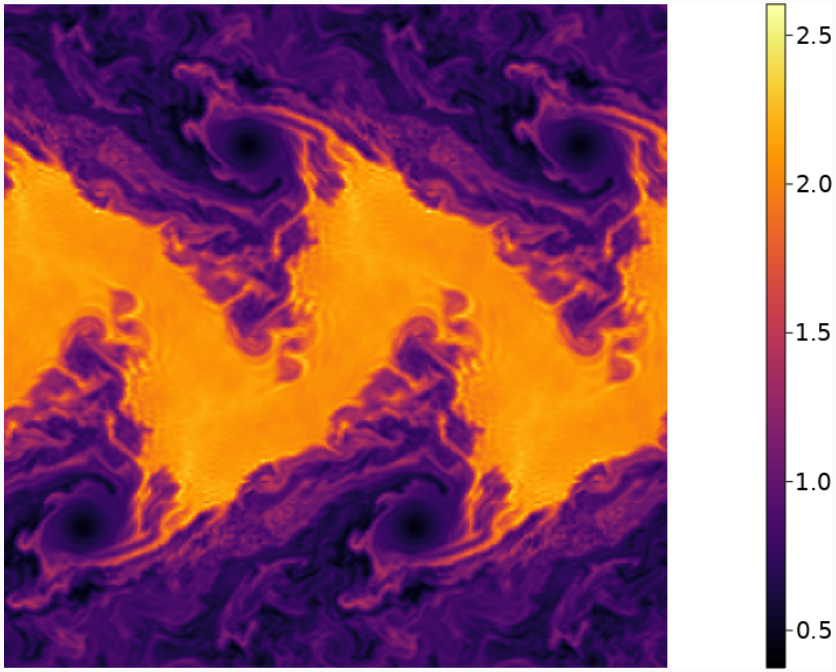

(a) Degree $N = 3$ and a 64×64 mesh.

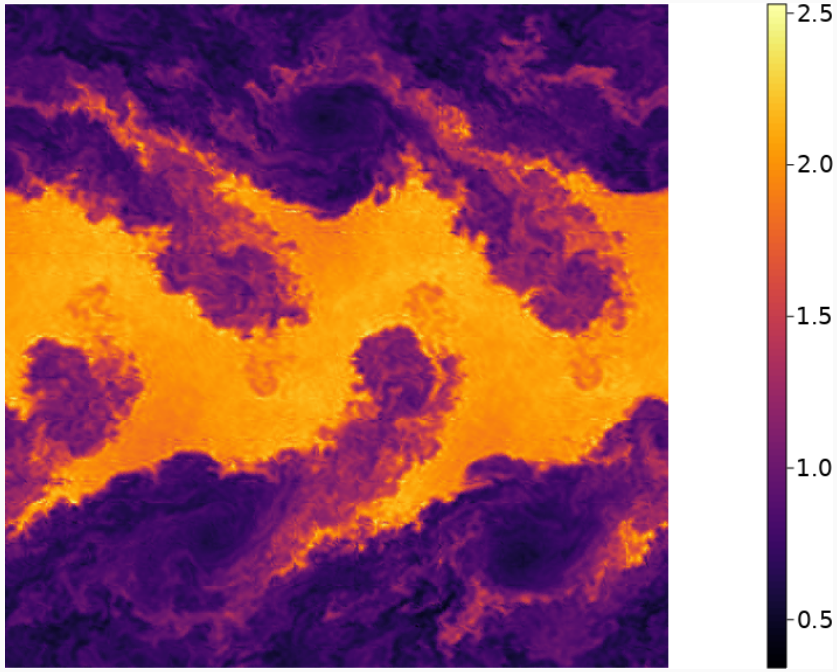

(b) Degree $N = 7$ and a 32×32 mesh.

Density at time $T = 10$ for the Kelvin-Helmholtz instability using an entropy stable DG method with entropy projection.

Differences in ESDG robustness for compressible Euler

Solver \ Degree	1	2	3	4	5	6	7
Collocation	15	4.81	3.77	4.43	3.74	3.37	3.64
Entropy projection	15	15	15	15	15	15	15

$N_{\text{cells}} = 16$

Solver \ Degree	1	2	3	4	5	6	7
Collocation	15	4.12	3.65	4.27	3.54	3.66	3.56
Entropy projection	15	15	15	15	15	15	15

$N_{\text{cells}} = 32$

End times for the Kelvin-Helmholtz instability on quadrilateral meshes. Blue indicates stable simulations, while red indicate crashes.

Differences in ESDG robustness for compressible Euler

Solver \ Degree	1	2	3	4	5	6
Collocation	15	3.98	3.44	2.99	2.94	3.13
Entropy projection	15	15	15	15	15	15

$N_{\text{cells}} = 16$

Solver \ Degree	1	2	3	4	5	6
Collocation	3.919	3.45	3.19	2.96	3.06	3.27
Entropy projection	15	15	15	15	15	15

$N_{\text{cells}} = 32$

End times for the Kelvin-Helmholtz instability on triangular meshes. Blue indicates stable simulations, while red indicate crashes.

Similar behavior for Rayleigh-Taylor, Richtmeyer-Meshkov

(a) $t = 1.25$ **(b)** $t = 1.5$ **(c)** $t = 1.75$ **(d)** $t = 2$ **(e)** $t = 2.5$

Rayleigh-Taylor instability: $N = 3$ entropy projection DG, 32×128 elements.

Similar behavior for Rayleigh-Taylor, Richtmeyer-Meshkov

Solver \ Degree	1	2	3	4	5	6	7
Collocation	3.67	3.4	3.33	3.26	3.11	3.03	3.04
Entropy projection	15	15	15	15	15	15	15

RTI, quadrilateral mesh, $N_{\text{cells}} = 16$

Solver \ Degree	1	2	3	4	5	6	7
Collocation	4.00	3.14	3.44	3.16	3.03	2.97	2.98
Entropy projection	15	15	15	15	15	15	15

RTI, quadrilateral mesh, $N_{\text{cells}} = 32$

End times for the Rayleigh-Taylor instability. Blue indicates stable simulations, while red indicate crashes.

Similar behavior for Rayleigh-Taylor, Richtmeyer-Meshkov

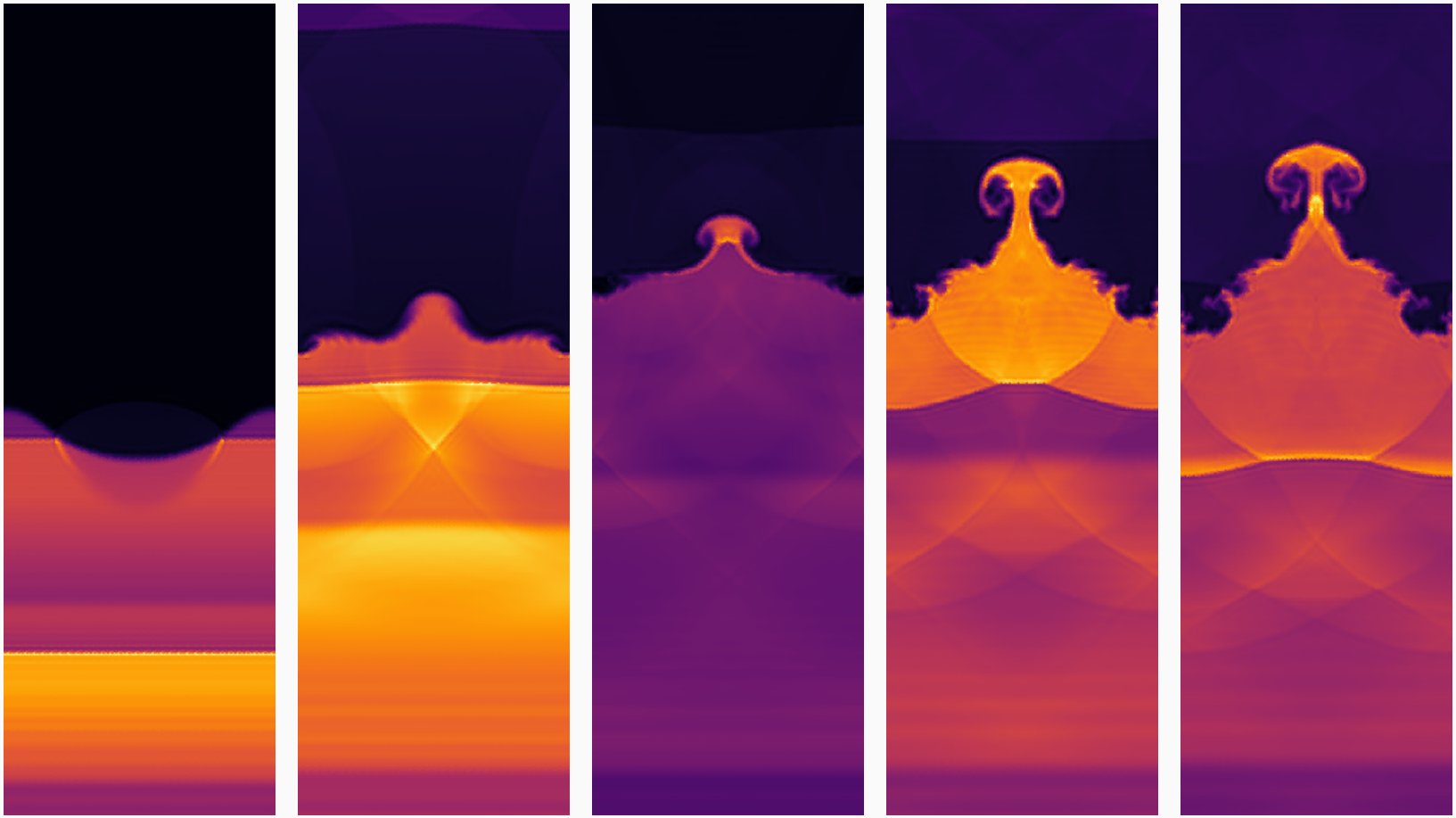

(a) $t = 7.5$ **(b)** $t = 15$ **(c)** $t = 20$ **(d)** $t = 25$ **(e)** $t = 27.5$

Richtmeyer-Meshkov instability using $N = 3$ entropy projection DG with 32×96 elements. Entropy projection is stable up to $T = 50$; entropy stable collocation crashes at $T \approx 20.1$.

Similar behavior for Rayleigh-Taylor, Richtmeyer-Meshkov

Solver \ Degree	1	2	3	4	5	6	7
Collocation	30	30	27.96	24.94	8.851	8.853	8.85
Entropy projection	30	30	30	30	30	30	30

RMI, quadrilateral mesh, $N_{\text{cells}} = 16$

Solver \ Degree	1	2	3	4	5	6	7
Collocation	30	25.52	23.34	8.759	7.808	7.014	7.01
Entropy projection	30	30	30	30	30	30	30

RMI, quadrilateral mesh, $N_{\text{cells}} = 32$

End times for the Richtmeyer-Meshkov instability. Blue indicates stable simulations, while red indicate crashes.

Robustness depends on the Atwood number

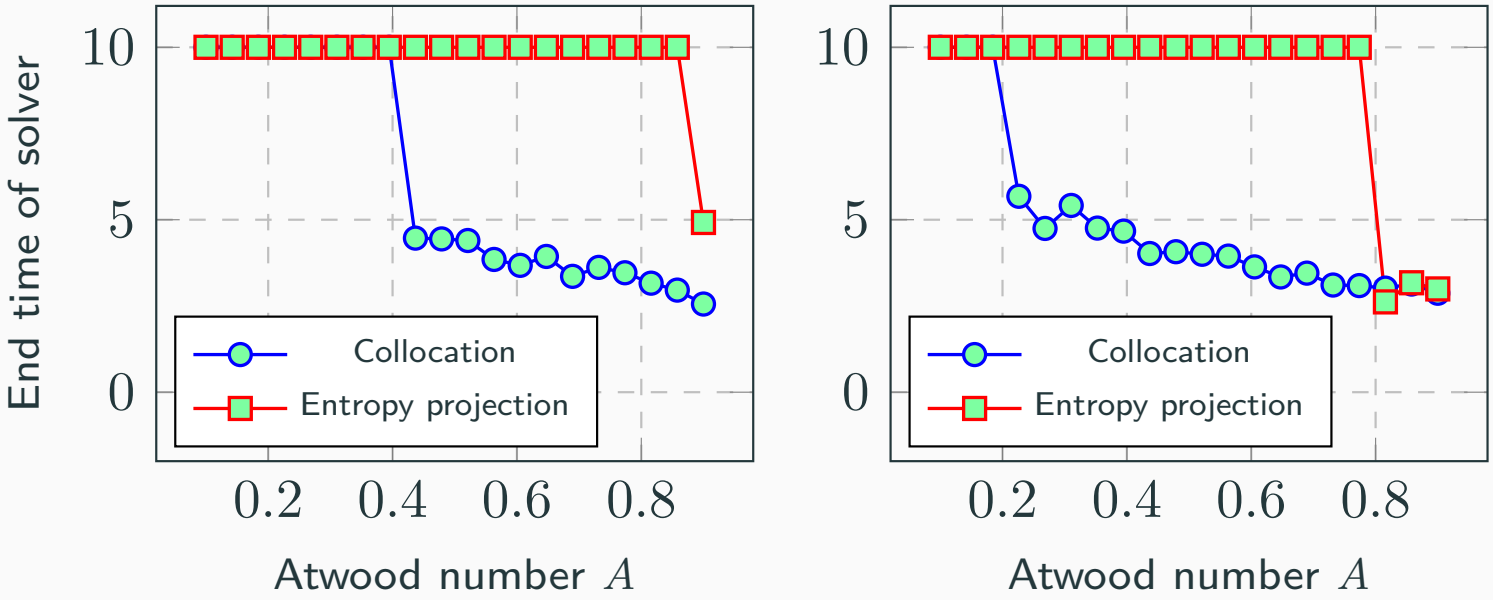

(a) $N = 3$, 32×32 quad mesh **(b)** $N = 7$, 16×16 quad mesh

- Entropy stable collocation DG is robust when density is near-constant, but crashes at higher Atwood numbers

$$A = (\rho_2 - \rho_1)/(\rho_1 + \rho_2), \qquad A \in [0, 1).$$

- Entropy projection is stable up to $A \approx .8$.

Why the difference in robustness?

CAN YOU SPOT ALL 5 DIFFERENCES BETWEEN THESE TWO discretizations ?

- Both are entropy stable, but Gauss collocation increases quadrature accuracy (reduces aliasing).
- Gauss introduces interface corrections and entropy projection.

Figures courtesy of https://bcsrc.ca/kids/spot-the-difference/.

Why would the entropy projection improve robustness?

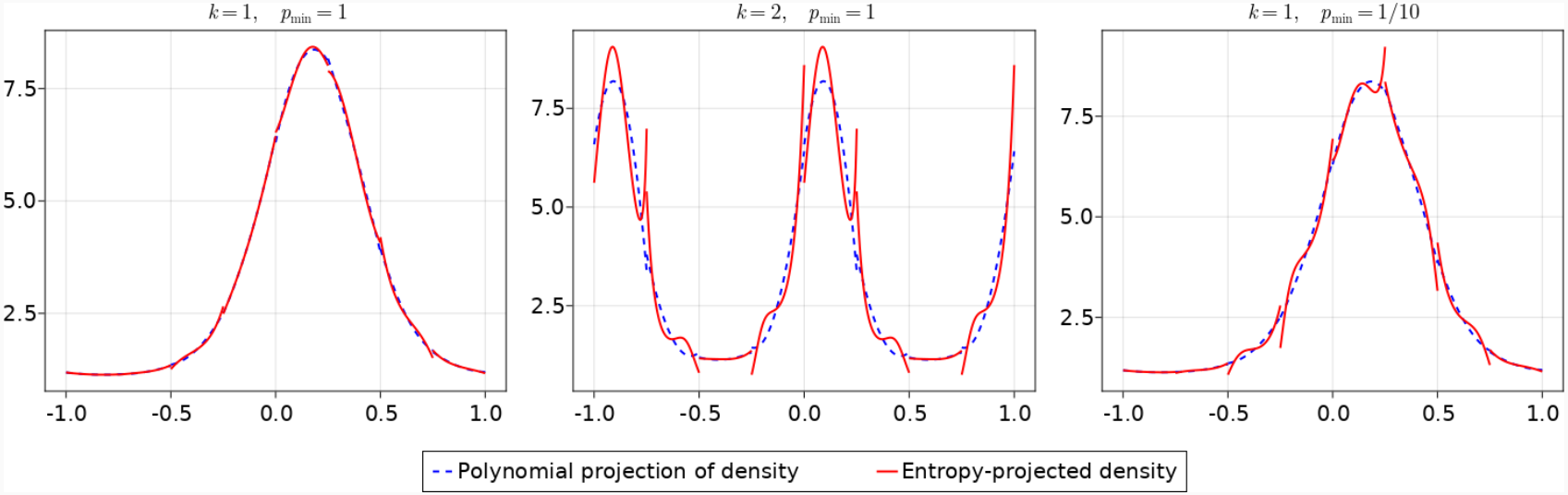

Some clues: entropy projection uses L^2 projection of entropy variables, amplifies effects of under-resolution and near-zero density or pressure.

Evolution of differences between the conservative variables and entropy projected variables

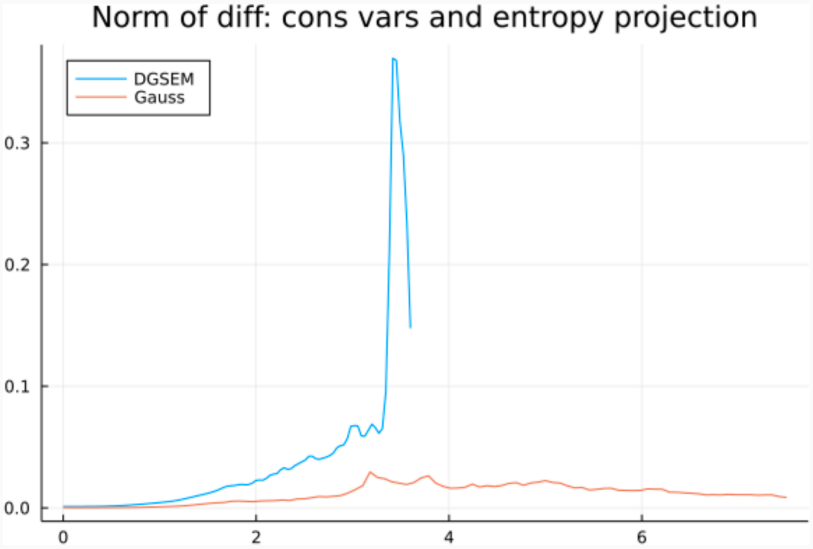

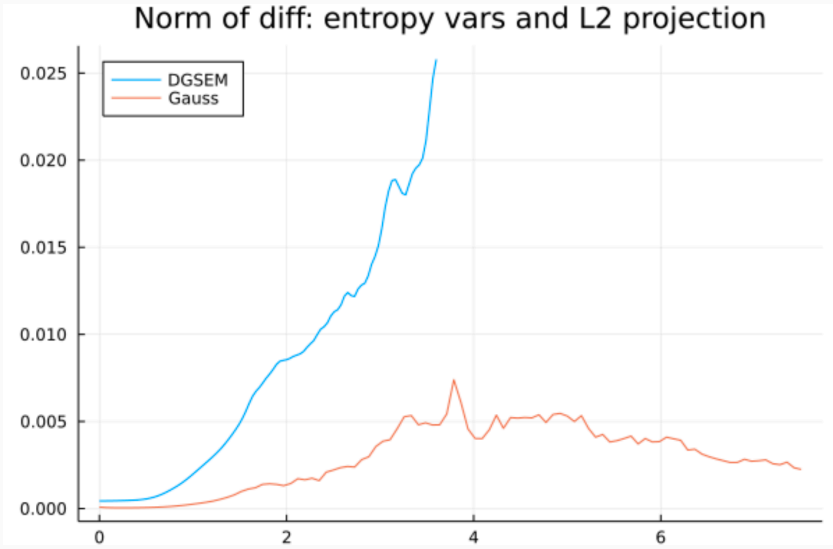

Difference over time between the conservative and entropy projected variables $\|\widetilde{\boldsymbol{u}} - \boldsymbol{u}\|_{L^2}$ for collocation and entropy projection schemes.

If $\widetilde{\boldsymbol{u}} \approx \boldsymbol{u}$, the mapping between conservative and entropy variables is well-posed $\Longrightarrow$ the density and pressure are positive?

Why not just use shock capturing and positivity limiting?

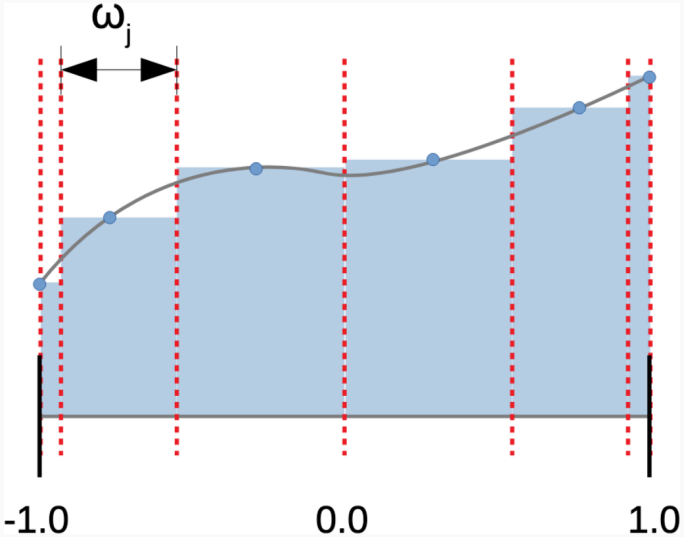

Interpretation of Lobotto nodes as a sub-cell finite volume grid.

We compare entropy projection DG to two state-of-the-art schemes:

- DGSEM-SC-PP: very light entropy stable shock capturing + Zhang-Shu positivity limiting.
- DGSEM-subcell: positivity and shock capturing using subcell convex limiting.

Hennemann, Ruéda-Ramírez, Hindenlang, Gassner (2021). A provably entropy stable subcell shock capturing approach for high order split form DG for the compressible Euler equations.

Ruéda-Ramírez, Pazner, Gassner (2022, preprint). Subcell limiting strategies for DGSEM.

Application: under-resolved “turbulent” flows

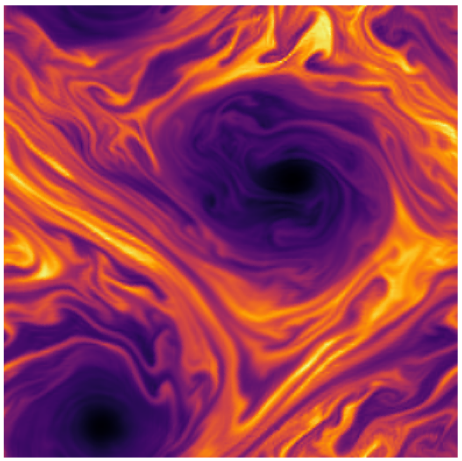

DGSEM-SC-PP density

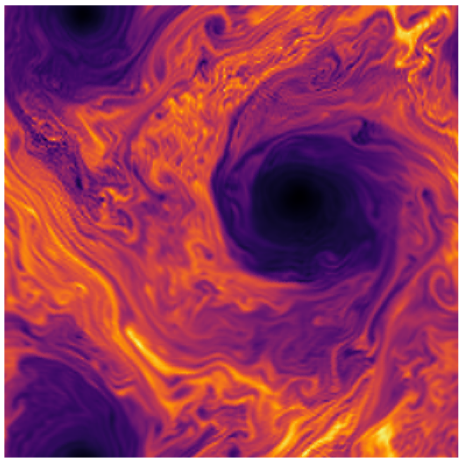

DGSEM-subcell density

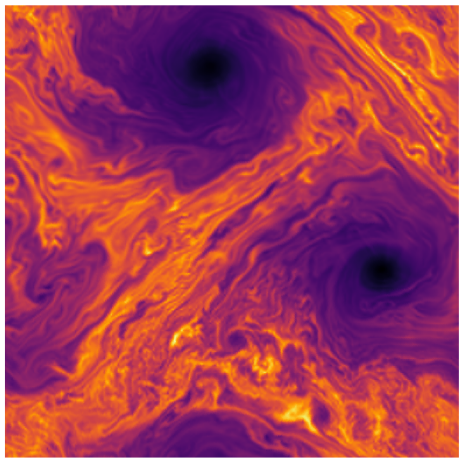

Gauss density

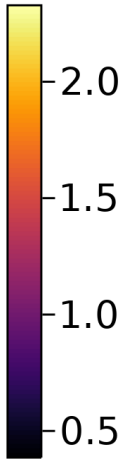

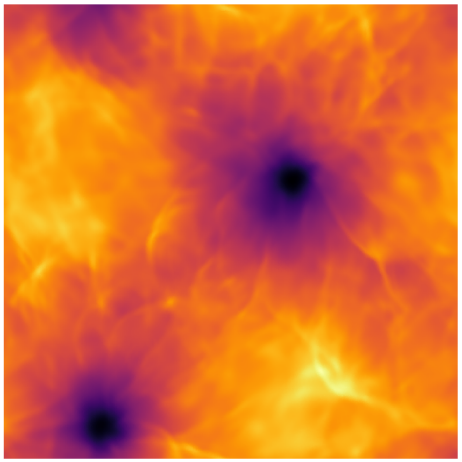

DGSEM-SC-PP pressure

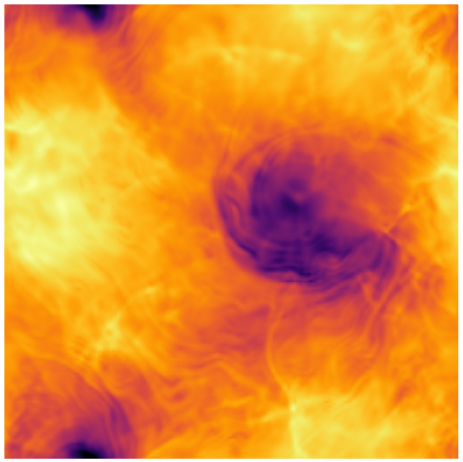

DGSEM-subcell pressure

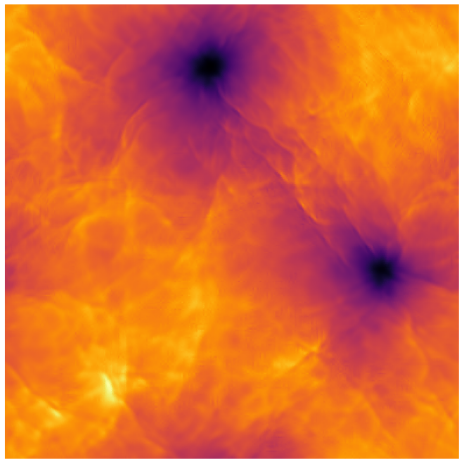

Gauss pressure

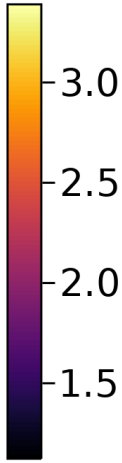

Application: under-resolved “turbulent” flows

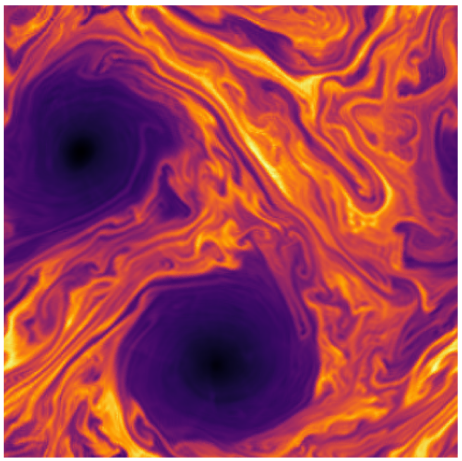

DGSEM-SC-PP density

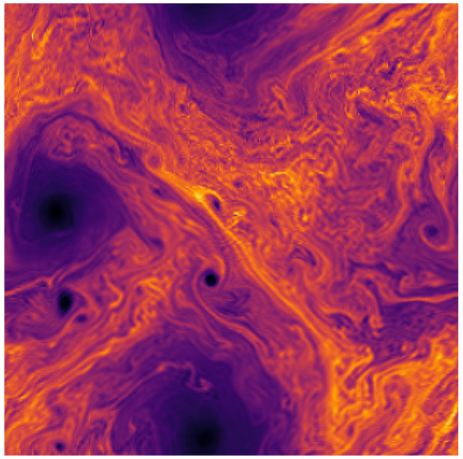

DGSEM-subcell density

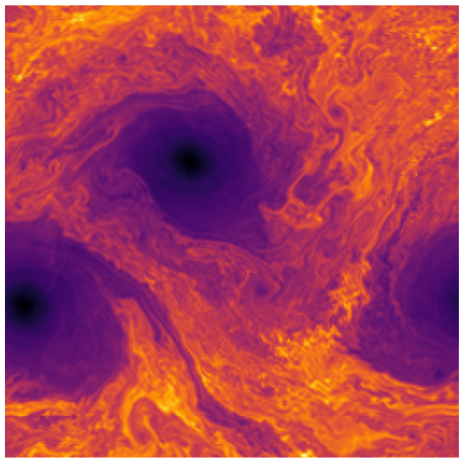

Gauss density

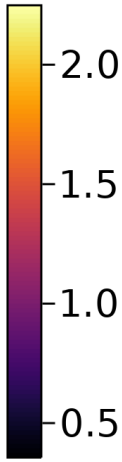

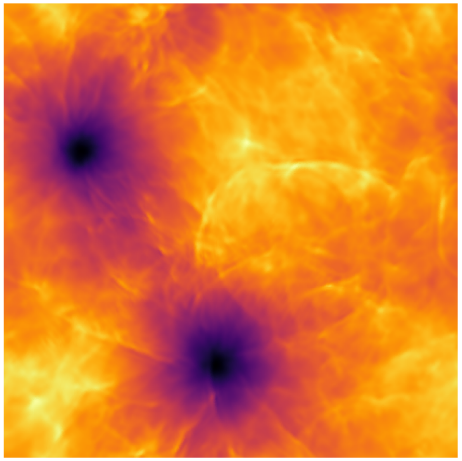

DGSEM-SC-PP pressure

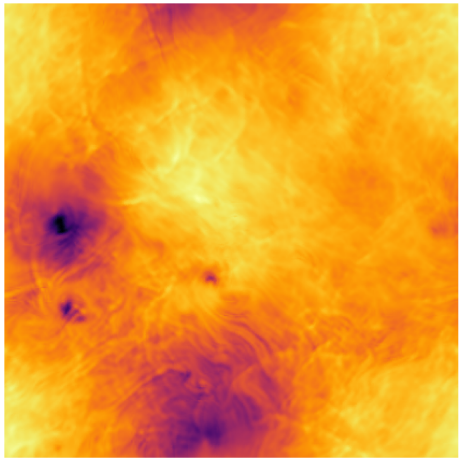

DGSEM-subcell pressure

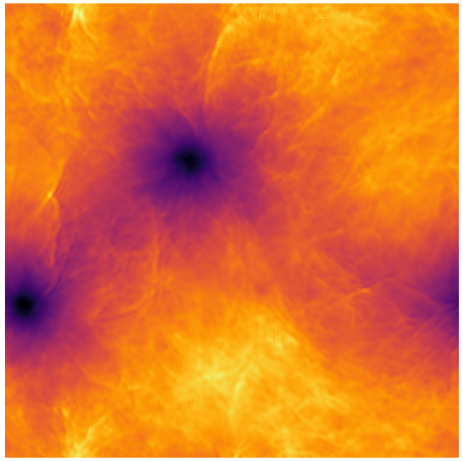

Gauss pressure

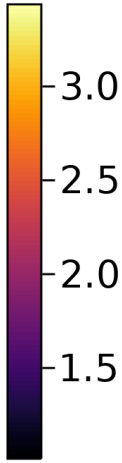

Under-resolved "turbulence" is sensitive to extra dissipation

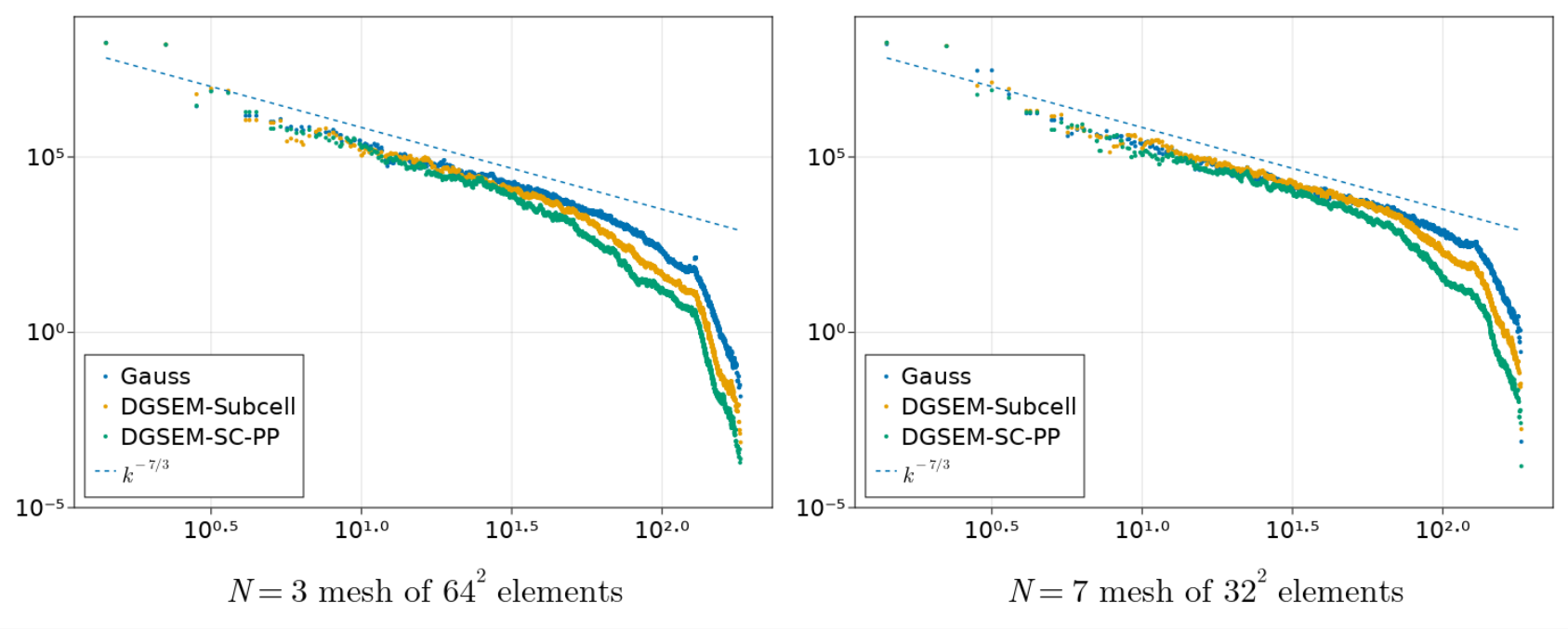

- Sample with $(N+1) \times$ number of elements points (uniformly spaced to avoid element interfaces) along each dimension.
- Compute Fourier modes of velocity weighted by $\sqrt{\rho}$, sum energy over "effective wavenumbers" for a 1D power spectra.

Conclusion

- Positivity preserving limiters enable robust entropy stable nodal DG simulations of compressible flow.
- The "entropy projection" seems to improves robustness for under-resolved flows (but we don't know why?).
- This work is supported by DMS-1943186.

Thank you! Questions?

Chan, Ranocha, Rueda-Ramírez, Gassner, Warburton (2022). *On the entropy projection and the robustness of high order entropy stable discontinuous Galerkin schemes for under-resolved flows*.

Lin, Chan, Tomas (2022). *A positivity preserving strategy for entropy stable discontinuous Galerkin discretizations of the compressible Euler and Navier-Stokes equations*.

Chan, Lin, Warburton (2021). *Entropy stable modal discontinuous Galerkin schemes and wall boundary conditions for the compressible Navier-Stokes equation*.

Additional slides

"Hybridization" for efficient interface coupling

- *Hybridized* SBP operators involve *both* volume/face nodes.

$$\mathbf{Q}_h = \frac{1}{2}\begin{bmatrix} \mathbf{Q} - \mathbf{Q}^T & \mathbf{E}^T\mathbf{B} \\ -\mathbf{B}\mathbf{E} & \mathbf{B} \end{bmatrix},$$

- Let $g(x)$ be a function. We can approximate $\frac{\partial g}{\partial x}$ via

$$\frac{\partial g}{\partial x} \approx \mathbf{M}^{-1}\begin{bmatrix} \mathbf{V}_q \\ \mathbf{V}_f \end{bmatrix}^T \mathbf{Q}_h \begin{bmatrix} g(\mathbf{x}_q) \\ g(\mathbf{x}_f) \end{bmatrix},$$

  where $\mathbf{x}_q, \mathbf{x}_f$ are volume and face nodes, $\mathbf{V}_q, \mathbf{V}_f$ are volume and face interpolation matrices.

- Equivalent to adding error-reducing correction terms of the form "$\mathbf{E}\boldsymbol{f}(\mathbf{u}) - \boldsymbol{f}(\mathbf{E}\mathbf{u})$".

Entropy stable schemes using hybridized SBP operators

- Replace SBP operator with hybridized SBP operator

$$\mathbf{M}\frac{\mathrm{d}\mathbf{u}}{\mathrm{dt}} + 2\left(\mathbf{Q}\circ\mathbf{F}\right)\mathbf{1} + \mathbf{E}^T\mathbf{B}\left(\mathbf{f}^* - \boldsymbol{f}(\mathbf{u})\right) = 0.$$

- $\mathbf{F}$ is the matrix of flux evaluations using solution values at *both* volume and face nodes + entropy projection:

$$\mathbf{F}_{ij} = \boldsymbol{f}_S\left(\widetilde{\mathbf{u}}_i, \widetilde{\mathbf{u}}_j\right), \qquad \widetilde{\mathbf{u}} = \text{ evaluate } \boldsymbol{u}\left(\Pi_N \boldsymbol{v}(\mathbf{u})\right).$$

- Entropy stable if $\mathbf{Q}_h\mathbf{1} = \mathbf{0}$ (true under weak conditions on quadrature accuracy).

Chan (2019). *Skew-symmetric entropy stable modal discontinuous Galerkin formulations.*

Chan (2018). *On discretely entropy conservative and entropy stable discontinuous Galerkin methods.*

Entropy stable schemes using hybridized SBP operators

- Replace SBP operator with hybridized SBP operator

$$\mathbf{M}\frac{\mathrm{d}\mathbf{u}}{\mathrm{dt}} + 2\begin{bmatrix}\mathbf{V}_q \\ \mathbf{V}_f\end{bmatrix}^T (\mathbf{Q}_h \circ \mathbf{F})\,\mathbf{1} + \mathbf{V}_f^T\mathbf{B}\left(\mathbf{f}^* - \boldsymbol{f}(\mathbf{u})\right) = 0.$$

- $\mathbf{F}$ is the matrix of flux evaluations using solution values at *both* volume and face nodes + entropy projection:

$$\mathbf{F}_{ij} = \boldsymbol{f}_S\left(\widetilde{\mathbf{u}}_i, \widetilde{\mathbf{u}}_j\right), \qquad \widetilde{\mathbf{u}} = \text{ evaluate } \boldsymbol{u}\left(\Pi_N \boldsymbol{v}(\mathbf{u})\right).$$

- Entropy stable if $\mathbf{Q}_h\mathbf{1} = \mathbf{0}$ (true under weak conditions on quadrature accuracy).

Chan (2019). *Skew-symmetric entropy stable modal discontinuous Galerkin formulations.*

Chan (2018). *On discretely entropy conservative and entropy stable discontinuous Galerkin methods.*

Entropy stable schemes using hybridized SBP operators

- Replace SBP operator with hybridized SBP operator

$$\mathbf{M}\frac{\mathrm{d}\mathbf{u}}{\mathrm{dt}} + 2\begin{bmatrix}\mathbf{V}_q \\ \mathbf{V}_f\end{bmatrix}^T (\mathbf{Q}_h \circ \mathbf{F})\,\mathbf{1} + \mathbf{V}_f^T\mathbf{B}\left(\mathbf{f}^* - \boldsymbol{f}(\mathbf{u})\right) = 0.$$

- $\mathbf{F}$ is the matrix of flux evaluations using solution values at *both* volume and face nodes + entropy projection:

$$\mathbf{F}_{ij} = \boldsymbol{f}_S\left(\widetilde{\mathbf{u}}_i, \widetilde{\mathbf{u}}_j\right), \qquad \widetilde{\mathbf{u}} = \text{ evaluate } \boldsymbol{u}\left(\Pi_N \boldsymbol{v}(\mathbf{u})\right).$$

- Entropy stable if $\mathbf{Q}_h\mathbf{1} = \mathbf{0}$ (true under weak conditions on quadrature accuracy).

Chan (2019). *Skew-symmetric entropy stable modal discontinuous Galerkin formulations.*

Chan (2018). *On discretely entropy conservative and entropy stable discontinuous Galerkin methods.*

Entropy stable schemes using hybridized SBP operators

- Replace SBP operator with hybridized SBP operator

$$\mathbf{M}\frac{\mathrm{d}\mathbf{u}}{\mathrm{dt}} + 2\begin{bmatrix}\mathbf{V}_q \\ \mathbf{V}_f\end{bmatrix}^T (\mathbf{Q}_h \circ \mathbf{F})\,\mathbf{1} + \mathbf{V}_f^T\mathbf{B}\left(\mathbf{f}^* - \boldsymbol{f}(\mathbf{u})\right) = 0.$$

- $\mathbf{F}$ is the matrix of flux evaluations using solution values at *both* volume and face nodes + entropy projection:

$$\mathbf{F}_{ij} = \boldsymbol{f}_S\left(\widetilde{\mathbf{u}}_i, \widetilde{\mathbf{u}}_j\right), \qquad \widetilde{\mathbf{u}} = \text{ evaluate } \boldsymbol{u}\left(\Pi_N \boldsymbol{v}(\mathbf{u})\right).$$

- Entropy stable if $\mathbf{Q}_h\mathbf{1} = \mathbf{0}$ (true under weak conditions on quadrature accuracy).

Chan (2019). *Skew-symmetric entropy stable modal discontinuous Galerkin formulations.*

Chan (2018). *On discretely entropy conservative and entropy stable discontinuous Galerkin methods.*

Estimated cost for DGSEM and Gauss

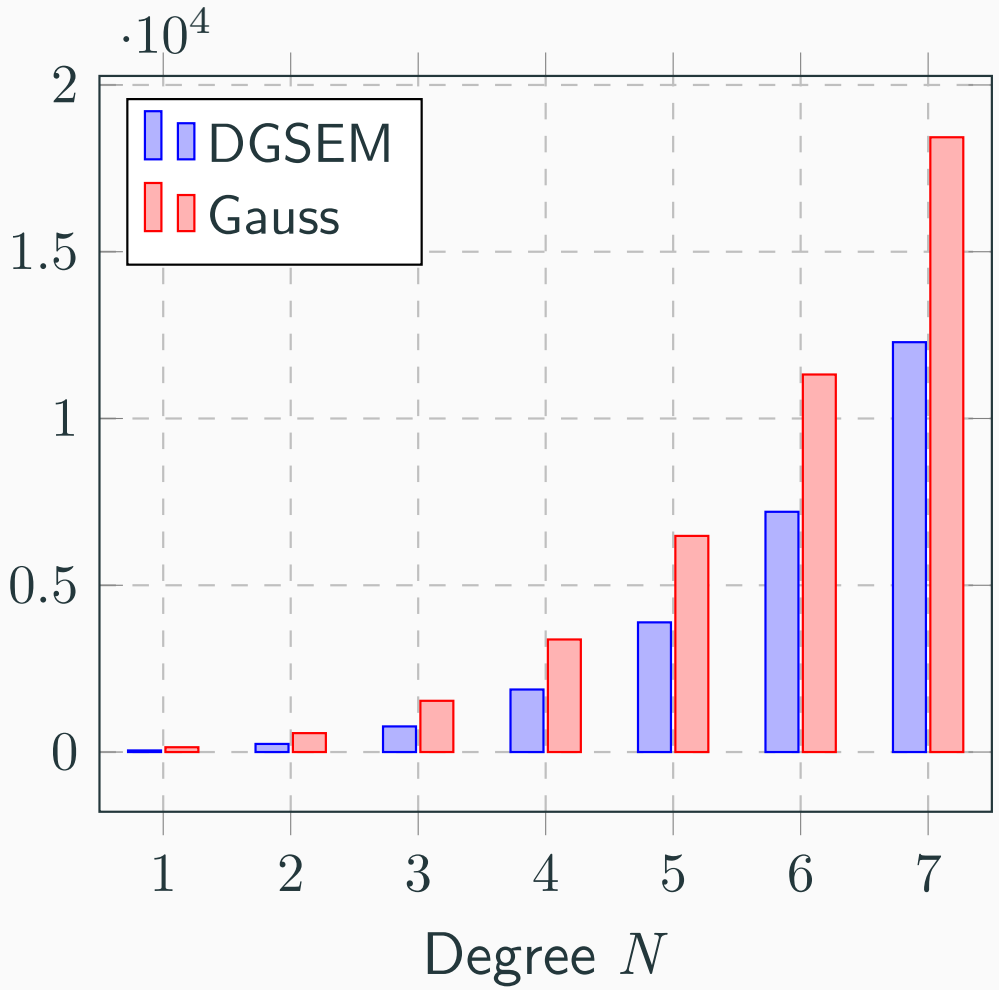

Figure 1: Comparison of 3D entropy stable DGSEM and entropy stable Gauss collocation in terms of two-point numerical flux evaluations.

Actual cost comparison for DGSEM and Gauss

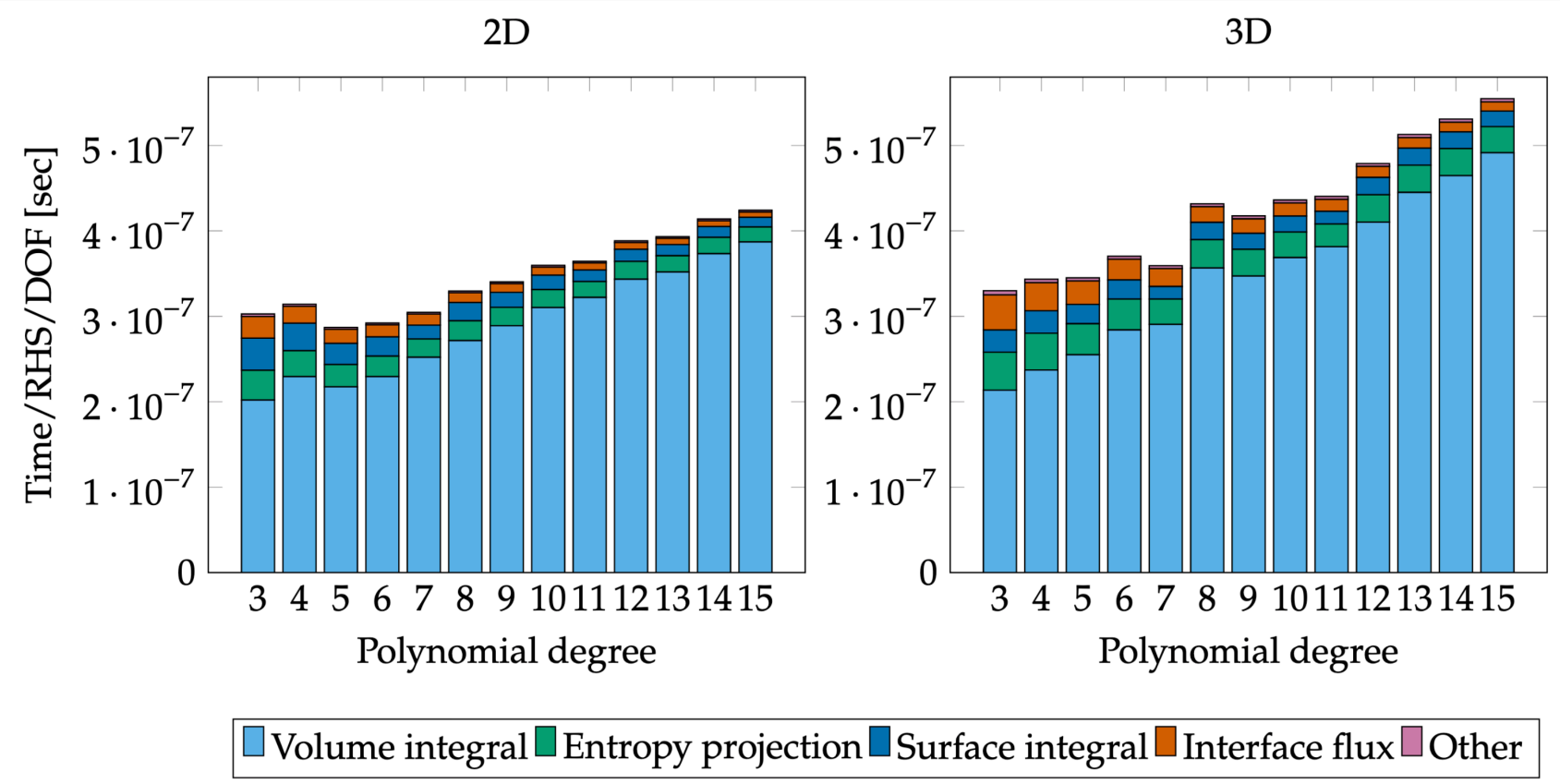

Performance index (PID) for entropy stable Gauss collocation.

Cost comparison of different implementations

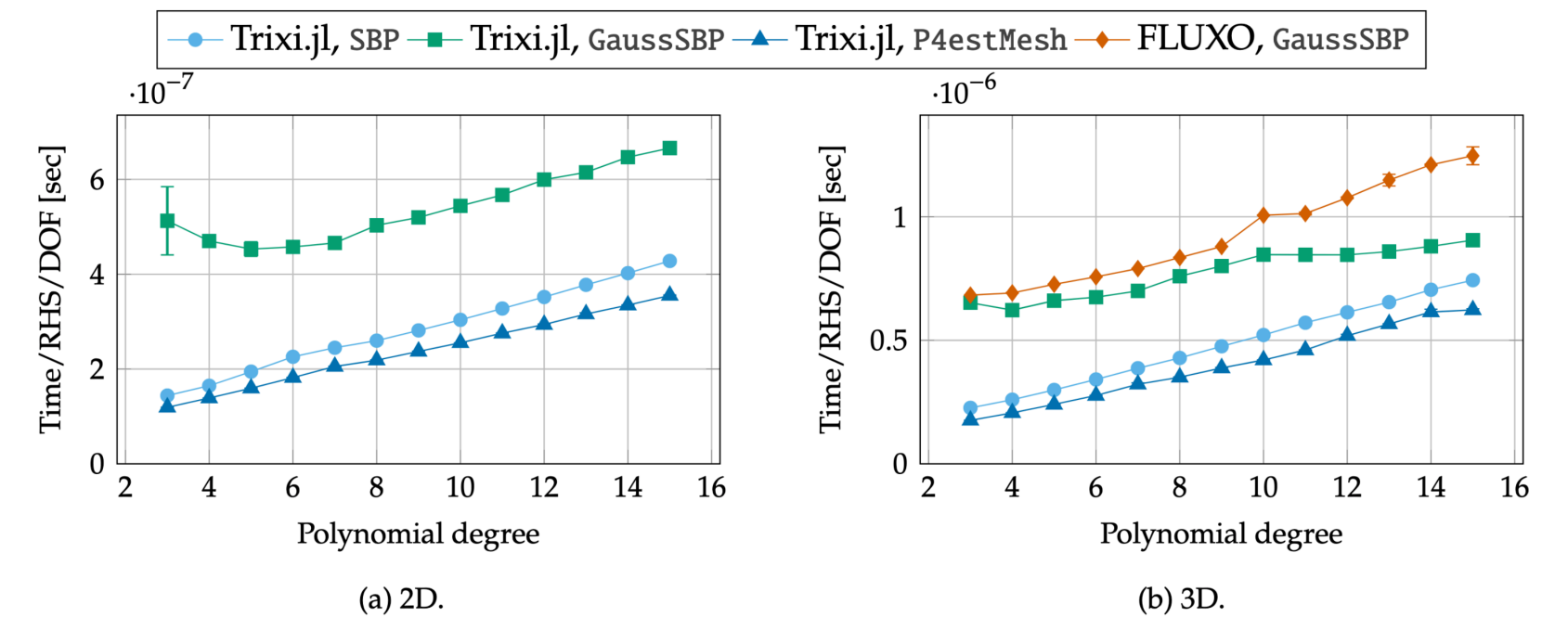

Runtime per RHS evaluation for different implementations of entropy stable DGSEM and Gauss collocation.

Does the entropy projection also help "bad" DG schemes?

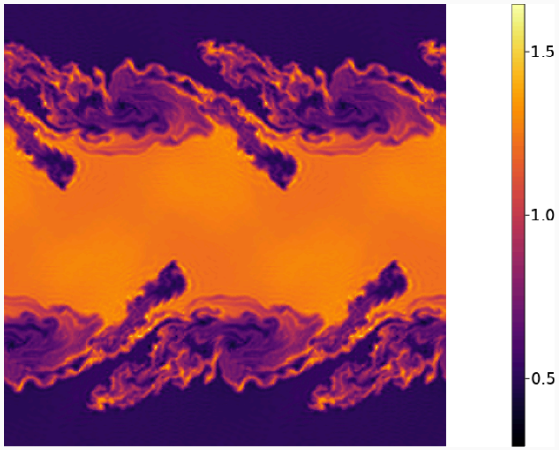

Entropy stable Gauss collocation

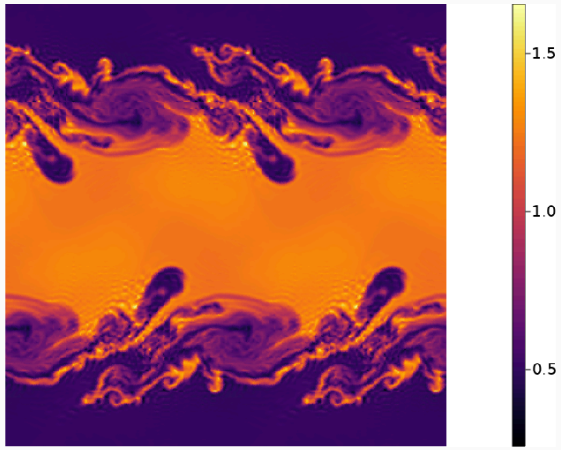

DGSEM with face-based entropy projection

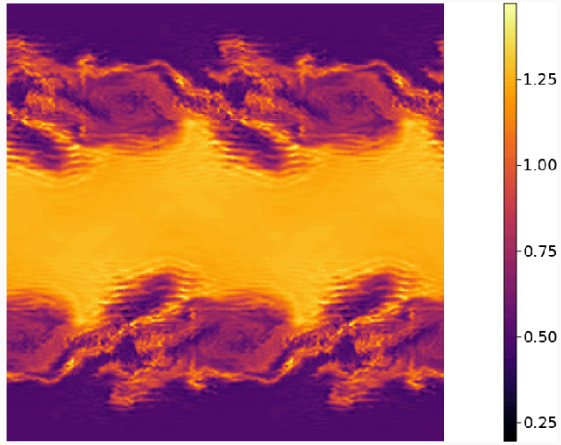

DGSEM with volume-based entropy projection

Degree $N = 3$ and 64×64 grid Kelvin-Helmholtz simulations at $T = 5$.
All methods run until $T = 25$, while DGSEM crashes at $T \approx 3.5$.

"Variant" schemes introduce entropy projection, but have similar or lower quadrature accuracy compared with DGSEM.

Improved robustness is not due to interface dissipation

Solver \ Degree	1	2	3	4	5	6	7
Collocation	20	20	20	20	6.035	5.29	5.02
Entropy projection	20	20	20	20	20	20	20

$$N_{\text{cells}} = 8^3$$

End times for entropy *conservative* simulations of the Taylor-Green vortex on hex meshes. Blue indicates stable simulations, while red indicate crashes.

We observe differences in robustness even for *entropy conservative* schemes (no entropy dissipation).

Improved robustness is not (only) due to quadrature accuracy

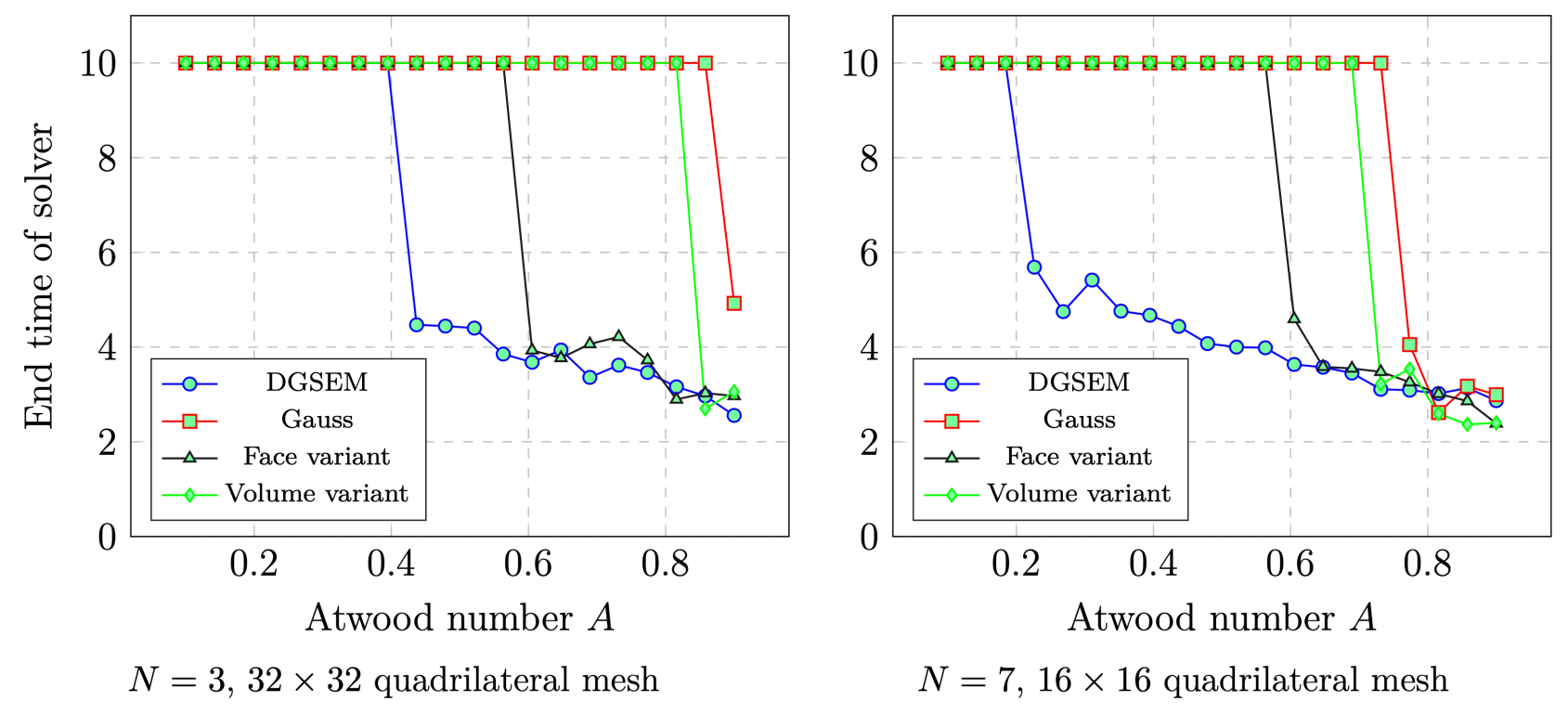

Entropy projection is not the only factor: "bad" entropy projection variant schemes improve robustness, but not as much.